CHALMERS
UNIVERSITY OF TECHNOLOGY

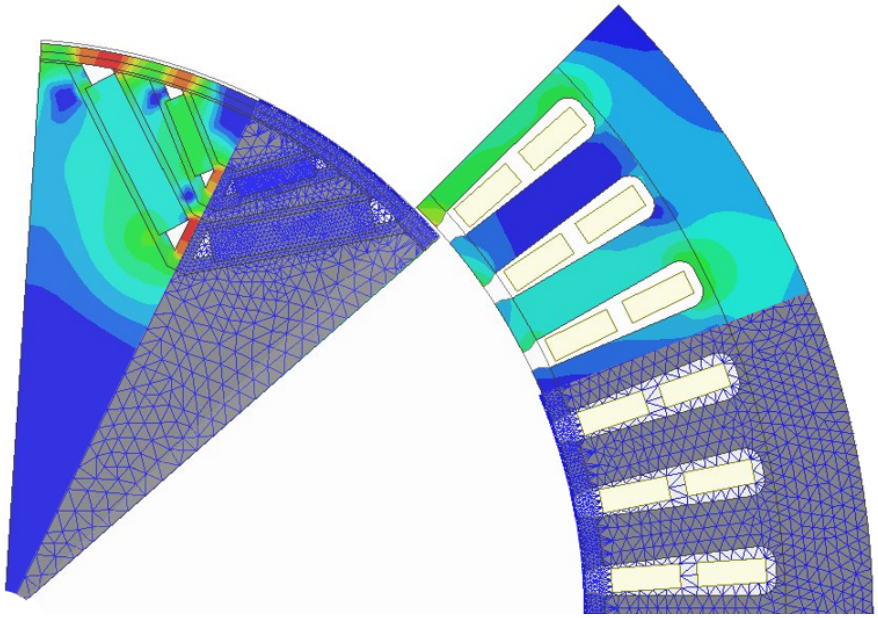

Iron Loss Modelling for a Permanent Magnet Synchronous Motor

An analytical comparison of iron loss modelling in time and frequency domain for different feeding techniques.

Master's thesis in Electrical Power Engineering

Edo Campara
Anes Solakovic

Department of Electrical Engineering
CHALMERS UNIVERSITY OF TECHNOLOGY
Gothenburg, Sweden 2020

Master's thesis 2020

Iron Loss Modelling for a Permanent Magnet Synchronous Motor

An analytical comparison of iron loss modelling in time and frequency domain for different feeding techniques.

Edo Campara
Anes Solakovic

CHALMERS
UNIVERSITY OF TECHNOLOGY

Department of Electrical Engineering
Division of Electrical Power Engineering
Chalmers University of Technology
Gothenburg, Sweden 2020

Iron Loss Modelling for a Permanent Magnet Synchronous Motor
An analytical comparison of iron loss modelling in time and frequency domain for different feeding techniques.
EDO CAMPARA
ANES SOLAKOVIC

Supervisor: Elisabet Jansson, Volvo Cars Corporation
Examiner: Thorbjörn Thiringer, Electrical Power Engineering

Master's Thesis 2020
Department of Electrical Engineering
Division of Electrical Power Engineering
Chalmers University of Technology
SE-412 96 Gothenburg
Telephone +46 31 772 1000

Cover: Cross-section of a permanent magnet synchronous motor model visualizing the magnetic flux and the adapted mesh.

Typeset in LaTeX
Printed by Chalmers Reproservice
Gothenburg, Sweden 2020

Iron Loss Modelling for a Permanent Magnet Synchronous Motor
An analytical comparison of iron loss modelling in time- and frequency domain for different feeding techniques.
EDO CAMPARA
ANES SOLAKOVIC
Department of Electrical Power Engineering
Chalmers University of Technology

Abstract

Iron loss modeling is a complex challenge in the applications of electrical machines. In this project, an analytical comparison of the calculation of iron losses in a time-domain model using the finite element method program ANSYS Maxwell to the calculation of losses in two frequency-domain models is performed. The comparison treats three different feeding techniques in three operating points for a model of a permanent magnet synchronous motor. In addition, voltage and switched voltage feeding are implemented, and a tool where other iron loss models, than the one used in ANSYS Maxwell, can be evaluated is created.

Besides the important success of implementing multiple feeding techniques and other iron loss models, the analytical findings of this report indicate that operating points of higher velocities gave the highest losses, which was expected. The feeding technique with the highest losses was switched voltage, giving spikes in megawatt-order for the high frequent switching events. Finally, the losses of the modified frequency-domain mode, which gave consistent results in voltage- and current-feeding, indicate more reliable results in comparison with the initially used model in ANSYS Maxwell. For more certainty, all results have to be evaluated towards experimental data.

Keywords: Iron losses, PMSM, Ansys Maxwell, PWM, SPWM, frequency domain, time domain

Acknowledgements

The project was completed in collaboration with Volvo Cars at the Division of Electric Power Engineering at Chalmers University of Technology.

We would like to express our great appreciation to the department of Electrical Machine Design at Volvo Cars for the warm welcome and the opportunity to collaborate and use their facilities. We are particularly grateful for the assistance given by Elisabet Jansson, who has been our supervisor at Volvo Cars. Assistance provided by Elisabet was greatly appreciated and always of high value.

Furthermore, we would like to acknowledge the support given by Torbjörn Thiringer, who has been our academic supervisor from Chalmers and with his great experience highly contributed in keeping the project in the right direction.

Edo Campara & Anes Solakovic, Gothenburg, June 2020

Contents

1

Introduction

One of the most controversial topics of today is global warming and the widespread challenges that comes with it. The transportation sector is one of the most significant contributors to CO_2 emissions, and many car companies have started to take action towards emission-free transportation by rapidly increasing the market of electric vehicles. The performance of electric vehicles has shown to outcompete combustion engine vehicles in a high manner, except for the driving range where it still lags due to the low energy density in today's batteries. Thus, the optimization of the power losses is of high importance for the driving range in electric vehicles. To optimize the performance and to reduce the losses and correctly specify the exact driving range for a commercialized car, a good model of the losses is highly valuable for the analysis. This is strongly dependent on increasing the knowledge of the actual losses in electrical machines. The power losses in an electric machine can be divided into mechanical, copper, and iron losses. The latter have more complicated behavior and are therefore more complicated to model precisely. In addition, there is no existing method to directly measure the iron losses in an accurate and cost-efficient way [1]. On the other hand, today's finite element method (FEM) simulations allow sophisticated modeling and analysis of an electrical machine and its losses. There are some limitations to the modeling due to, for example, the manufacturing process of the soft magnetic material, which changes its characteristics and the harmonic content in inverter fed machines [1], which are difficult to include in the simulation. These limitations are often compensated for by multiplying the estimated losses with a correction factor that is obtained from previous prototype measurements [1].

1.1 Problem Definition

This report will focus on the modeling of iron losses in one of the most used motors for electric vehicles - the permanent magnet synchronous motor (PMSM). Firstly, sinusoidal voltage feeding will be implemented to the default iron loss model (Bertotti model) in the used FEM software, called ANSYS Maxwell. Secondly, the implementation of switched voltage feeding will be completed. At last, some modifications of the Bertotti model in frequency domain will be tried out, and the calculated iron losses will be compared depending on the type of voltage feeding and type of core loss model.

1.2 Aim

The project aims to study the behavior of the iron losses in a chosen PMSM for both sinusoidal and sinusoidal pulse width modulated (SPWM) feeding signals for multiple operating points by simulation in ANSYS Maxwell. From this, the final aim is to create a tool where various iron loss models can be implemented and evaluated in frequency domain.

1.3 Scope

As stated in the aim, the main objective of the project is to implement two types of voltage feeding on a chosen PMSM and to compare the losses with the usage of a different iron loss model in frequency domain. Further, the size of the PMSM will be fixed and chosen for battery electric vehicle applications. Different sizes, designs, or different types of electric machines will thus not be investigated. No experimental data will be collected nor used to verify the calculations. The report will neither focus on how the manufacturing process will affect the calculation of the iron losses; neither will the choice of core material in the motor be evaluated. Many of these aspects would be interesting to include in the analysis, yet they are placed outside of the scope because of the given time constrain.

2

Introduction to electrical drives systems

The following sections provides a broad theory to enable a better understanding of the coming chapters, where more focus will be directed to iron losses in detail. The chapter will include the system description of a battery electrical vehicle and at last the working principles of a PMSM and a switched voltage signal.

2.1 Battery electric vehicle (BEV) model

2.1.1 Dynamics

The purpose of vehicle dynamics is to describe the acting forces on a moving vehicle. These physics belong to classical mechanics and are essential during the design of a powertrain. From this type of study, an evaluation of the powertrains load and vehicle performance can be evaluated. Newton's second law states that the resulting forces of a moving body equal the mass times the acceleration, which is very central in vehicle dynamics. When it comes to on-road vehicles, mainly horizontal forces are of importance. Further, they can be divided into tractive and resistive forces, where the sooner contributes to the desired traction while the latter counteracts it, as in

$$F_{net} = ma = F_{tractive} - F_{resistive}[2] \tag{2.1}$$

Typically, the aerodynamic drag and rolling resistance are the main resistive forces, while the leading tractive force comes from the engine. Gravity can act as both a tractive and resistive force, depending on if the vehicle is driving uphill or downhill [2].

2.1.2 Powertrain

A typical electric vehicle powertrain consists of a drive system supplied by a rechargeable Lithium-ion battery pack. Here, a drive system with an AC machine will be considered, which is connected to the battery pack through a converter, as shown in figure 2.1. The converter's role is to reproduce AC voltage from the supplied DC voltage that is provided by the stored energy in the battery. The converter does this by switching the DC voltage on and off using a set of transistors, with the so-called pulse width modulation (PWM) method. This technique is described in more detail in section 2.10. Further, the electric machine converts electrical energy

to mechanical energy in the form of a rotating shaft. A gearbox with a reduction ratio is needed to slow down the very high speed of rotation of the machine, which usually reaches above 10 000 rpm. To provide some perspective on this value, it is worth to mention that 1200 rpm on a typical wheel of a car corresponds to a speed of 130 km/h. At last, the differential is used to enabling the wheels to spin at slightly different speeds when turning by splitting the torque on the right and left traction [2].

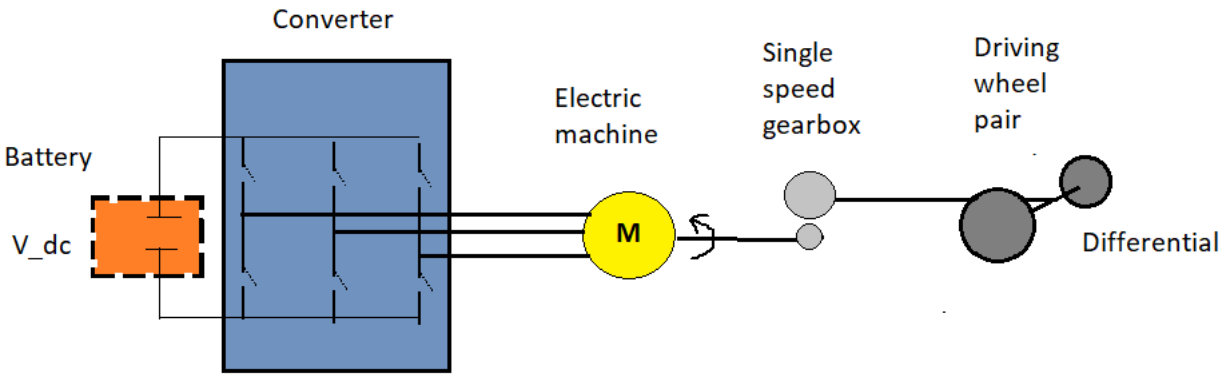

Figure 2.1: Illustration of a typical electric powertrain.

2.2 Working principle of PMSM

Permanent magnet synchronous motors (PMSM) as all-electric machines mainly consists of two parts - a fixed stator and a moving rotor. Both parts are usually built from a material with high magnetic permeability, i.e., a material with excellent magnetic conduction. Since most magnetic materials also are good conductors of electricity, the stator and rotor are built by stacking multiple thin lamination sheets together. In between each sheet, there are even thinner insulation layers to prevent current flow in axial direction [3]. To create movement in the rotor, a rotating magnetic field is created in the stator by driving alternating three-phase currents in the stator windings. The magnetic field in the rotor is provided by the magnets, which are mounted in such a way that these assure that the flux goes from north to south pole via the stator. The interaction of the stator and rotor fluxes results in a movement of the rotor. One could explain it as that the flux from the rotor "locks" into the rotating flux of the stator and starts to follow it in a synchronous rotating speed.

2.2.1 Operating range

An advantage of the PMSM is the wide operating range, which is very suitable for variable-speed drives. As can be seen in figure 2.2, the PMSM has a constant torque region and a region where the torque is ideally inversely proportional to the speed. The highest speed that can be achieved with maximum torque is called base speed. In figure 2.2, basespeed occurs at approx. 4200 rpm. It is defined by, besides being

the highest speed with maximum torque, is the speed where the back-EMF is equal to the applied voltage, and therefore the applied voltage can no longer be increased to increase the speed further. The relation is found as

$$V = \phi\omega, \tag{2.2}$$

where V is the applied voltage from the inverter, ϕ is the flux, and ω is the speed of the rotor.

When the basespeed is exceeded, the field-weakening region begins. To further increase the speed from base-speed and to keep a constant voltage according to (2.2), the field has to be decreased. This will, in turn, decrease the maximum available torque, which also is shown in figure 2.2.

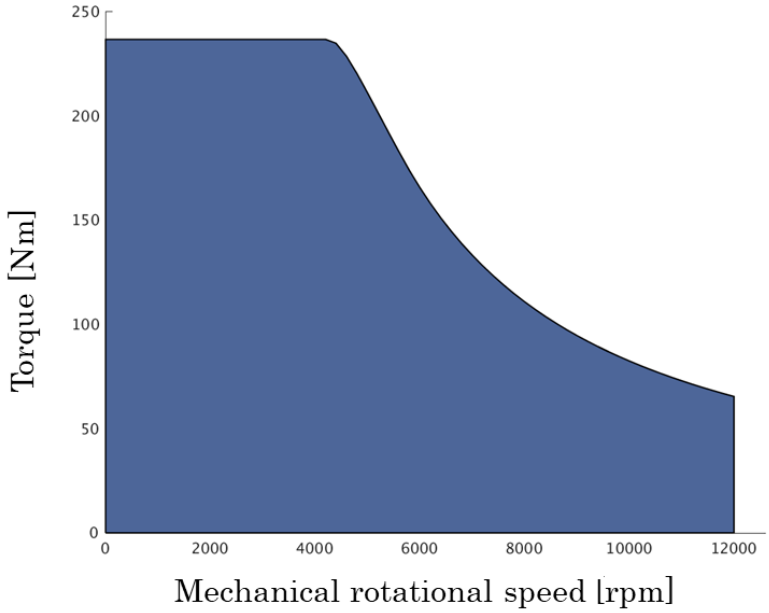

Figure 2.2: Typical operating range of a PMSM for automotive industry.

2.2.2 Park Transformation

In order to easier control the alternating signals in an electrical machine, a rotating coordinate system called "dq" is introduced. By using the Park transformation matrix presented in (2.3), the three-phase alternating variables can be represented on a coordinate system which is rotating at the same speed as the rotating field that is created by the currents. This results in a two DC-components commonly called i_d and i_q for the currents and u_d and u_q for the voltages. The d-axis is set in line with the magnet flux direction, and the q-axis is set to be orthogonal to the d-axis. [4]

$$\begin{bmatrix} i_d \\ i_q \end{bmatrix} = \frac{2}{3} \begin{bmatrix} cos\theta & cos(\theta - \frac{2\pi}{3} & cos(\theta - \frac{4\pi}{3}) \\ -sin\theta & -sin(\theta - \frac{2\pi}{3} & -sin(\theta - \frac{4\pi}{3} \end{bmatrix} \begin{bmatrix} i_a \\ i_b \\ i_c \end{bmatrix} \tag{2.3}$$

The d- and q-axis values can easily be used to calculate the magnitude and angle of the phase voltage by

$$U_{mag} = \sqrt{U_d^2 + U_q^2} \tag{2.4}$$

$$U_{angle} = \arctan(\frac{U_q}{U_d}), \tag{2.5}$$

where U_{mag} is the magnitude of the phase voltage and U_{angle} is the angle. The same calculations can be performed on the current.

2.2.3 Maximum Torque Per Ampere (MTPA)

Maximum torque per ampere is a control method that gives the lowest possible current magnitude for the desired torque. In the dq reference frame, the mathematical model of a PMSM can be expressed with the following expressions:

$$U_d = R_s i_d + L_d \frac{di_d}{dt} - \omega_r L_q i_q, \tag{2.6}$$

$$U_q = R_s i_q + L_q \frac{di_q}{dt} + \omega_r L_d i_d + \Psi_m \omega_r, \tag{2.7}$$

$$T_{em} = \frac{3}{2} p((L_d - L_q) i_d + \Psi_m) i_q, \tag{2.8}$$

where i_d and i_q are the d- and q-axis stator currents, R_s is the stator resistance, U_d and U_q are the d- and q-axis stator voltages, L_d and L_q are the d- and q-axis inductances, w_r is the electrical angular synchronous speed, T_{em} is the electromagnetic torque, p is the number of pole pairs and Ψ_m is the flux linkage of the permanent magnet [5]. By neglecting the voltage drop over the stator resistance, R_s, and using (2.6) and (2.7), the voltage and current limits can be defined as

$$I_{max}^2 \geq i_d^2 + i_q^2, \tag{2.9}$$

$$\frac{U_{max}^2}{\omega_r} \geq L_d^2 (i_d + \frac{\Psi_m}{L_d}) + L_q^2 i_q^2. \tag{2.10}$$

As shown in figure 2.3, the current limit has a shape of a circle with its center in origo, while the voltage limit has a shape of an ellipse due to saliency (i.e., $L_d \neq L_q$) with its center in $-\frac{\Psi_m}{L_d}$. One can also observe that the radius of the voltage limit ellipse decreases with increasing speed ($\omega_3 > \omega_2 > \omega_1$), meaning that the voltage becomes the limiting variable for higher speeds.

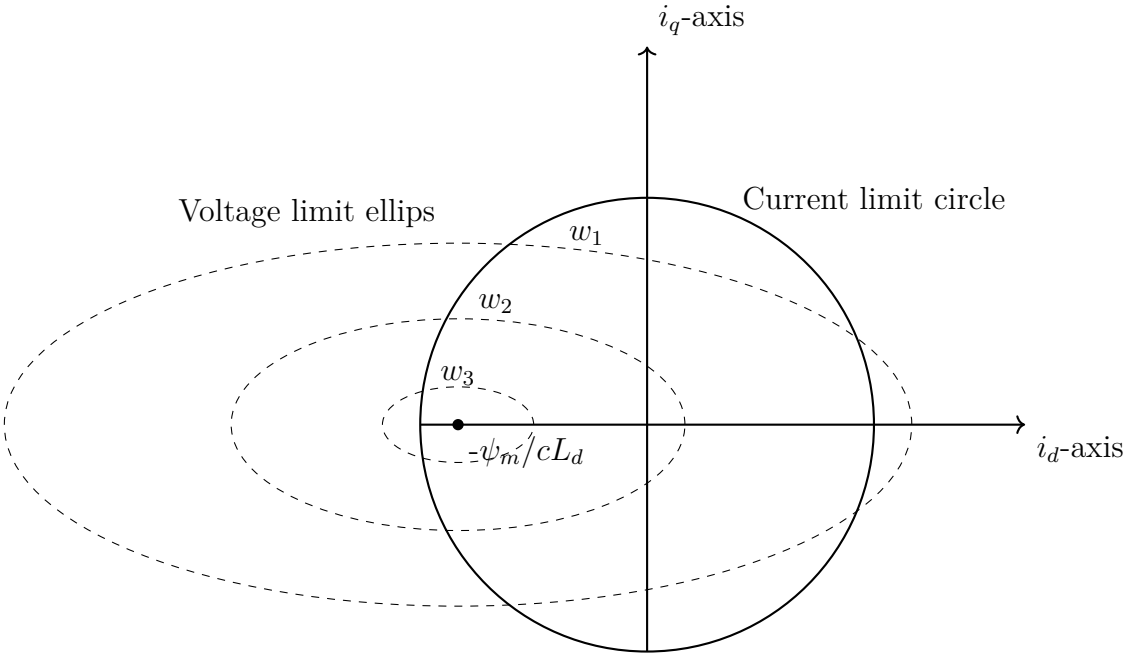

Figure 2.3: Illustration of the current and voltage constraints in the dq-current plane, where $w_3 > w_2 > w_1$.

To calculate the minimum current magnitude for a given electromagnetic torque, the torque equation (2.8) can first be expressed in terms of stator current magnitude and angle instead of i_d and i_q [5]. These equations are presented as

$$i_d = -Isin\gamma \tag{2.11}$$

$$i_q = Icos\gamma \tag{2.12}$$

$$T_{em} = \frac{3}{2}p(-\Psi_m Icos\gamma + \frac{1}{2}(L_d - L_q)I^2 sin2\gamma), \tag{2.13}$$

where I is the stator current magnitude, and γ is the stator current angle. Further, the rewritten torque equation (2.13) can be derived in terms of γ and set to zero ($\frac{dT_{em}}{d\gamma} = 0$) to find the angle of the stator current which ensures that a MTPA point is chosen for the desired torque. Solving γ from the derivation results in

$$\gamma = arcsin(\frac{-\Psi_m + \sqrt{\Psi_m^2 + 8I^2(L_q - L_d)^2}}{4I(L_q - L_d)^2}). \tag{2.14}$$

2.2.4 Losses in PMSM

With its high degree of efficiency, the electric machine is significantly better than the traditional combustion engine in converting energy to propel a vehicle forward. Despite this, energy optimization and thereby, reduction of losses are still of high interest due to the high costs of batteries and a low range of electric vehicles. The losses of a PMSM can be divided into three categories: mechanical losses, copper losses, and iron losses.

The main mechanical losses occure due to friction in bearings and in the air-friction in the airgap, more commonly know as windage. The mechanical losses are mainly affected by the geometry and the speed of the machine's rotating parts. The copper losses are depending on the current and resistance in the windings of the machine. In other words, the copper losses depend on the material and the size of the windings, but most importantly, on the operating current. Iron losses in electrical machines occur due to the time-varying electromagnetic field. Depending on the properties of the material and operating speed, the ratio between the iron losses to the total losses will differ. The iron losses will be a significant part of the total losses and cannot be neglected. For further information regarding iron losses, the reader is referred to section 3. Generally, for slower and larger machines, the copper losses are dominating while mechanical losses, due to friction, and iron losses, due to fast-changing magnetic field, take over with an increase in speed [3].

2.3 Switched Voltage

To supply an AC-machine in a vehicle with an appropriate voltage, an inverter between the battery and the AC-machine is needed. The inverter switches the DC-voltage from the battery on and off very quickly using transistors. A common method used for electrical drives applications is called sinusoidal pulse width modulation (SPWM). In a three-phase SPWM inverter, three reference sinusoidal signals at the desired frequency output and 120° displacement to each other are compared with a suitable high-frequency triangular carrier signal. When the reference signal is higher than the carrier signal, the upper leg in the inverter is turned on while the lower leg is turned off. When the reference signal becomes lower than the carrier signal, the lower leg is turned on instead. The output signal, presented in the bottom part of figure 2.4, will result in a pulse width modulated signal with the same fundamental frequency as the reference signal.

2.3.1 Modulation index

The ratio between the amplitude of the reference signal, $\hat{V}_{reference}$, and the amplitude of the carrier signal, $\hat{V}_{carrier}$, is defining the modulation index according to

$$m_a = \frac{\hat{V}_{reference}}{\hat{V}_{carrier}} \tag{2.15}$$

Typically, m_a is smaller or equal to one, giving a linear relationship between the input and output signal. However, if the amplitude of the reference signal exceeds the amplitude of the carrier signal, overmodulation will occur, resulting in a non-linear relationship for the input and output voltage. This non-linear behavior will give distorted output as well as unwanted harmonics, and the reference signal will no longer be able to be reproduced.

Just as the amplitude is modeled, the frequency will also have a dependency between the reference signal and the carrier signal. The frequency modulation m_f is defined

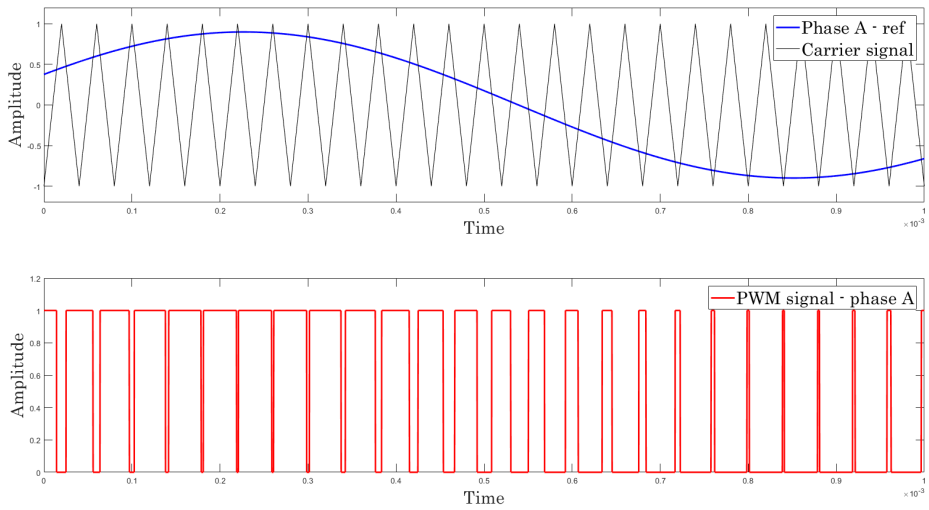

Figure 2.4: The upper figure showing the comparison of the sinusoidal reference signal in blue with a triangular carrier signal in black while the lower figure is showing the resulting sinusoidal pulse width modulated output signal in one phase.

as

$$m_f = \frac{f_{carrier}}{f_{reference}}, \tag{2.16}$$

where $f_{carrier}$ is the carrier signal frequency and $f_{reference}$ is the desired output frequency. The modulation index should be a multiple of three and an odd integer as well [6]. Generally, the carrier signal frequency should be as high as possible, since high-frequency harmonics are easier to filter out. In contrast, the switching losses for the inverter increase for higher frequencies. This creates a trade-off between switching losses and harmonics. Typically for electric vehicles, m_f is chosen to achieve a switching frequency of 10 kHz [7].

2.3.2 Third order harmonic injection

By injecting third-order harmonics to the reference signals, extending the range for avoiding over modulation and reducing stress on the switches is possible. The harmonic is added to each phase

$$\begin{aligned} V_A &= m_a(sin((\omega t) + \frac{1}{6}sin(3\omega t)) \\ V_B &= m_a(sin((\omega t + \frac{2\pi}{3}) + \frac{1}{6}sin(3\omega t + 3\frac{2\pi}{3})) \\ V_C &= m_a(sin((\omega t + +\frac{4\pi}{3}) + \frac{1}{6}sin(3\omega t + 3\frac{4\pi}{3})) \end{aligned} \tag{2.17}$$

Where V_A, V_B and V_C is the reference signal for each phase and m_a the amplitude modulation index, the addition of the third order, with the amplitude of one-sixth

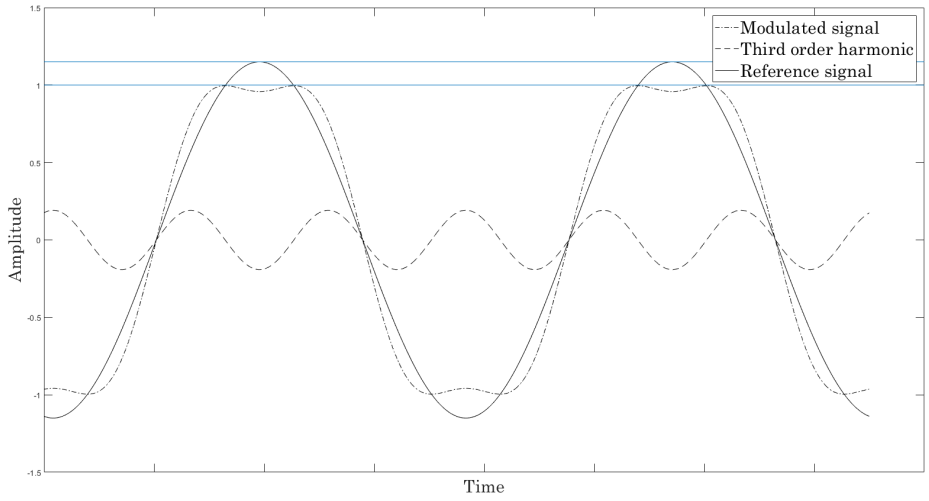

Figure 2.5: By injecting third-order harmonics, the amplitude peak value of the reference signal is flattened out, making it possible to utilize up to 15% more of the DC-link voltage.

of the reference signal, has the effect of flattening the top and reducing the peak value with a factor of 0.866 [8]. This makes it possible to extend the amplitude modulation index up to 1.15 without exceeding $\hat{V}_{carrier}$, which in return enables better utilization of the DC-link voltage. The effect of the injection on the reference signal is visualized in figure 2.5, while the resulting three-phase reference signals can be seen in figure 2.6. The main drawback with the injection of third-order harmonics is the limitation in gain and the small increase in total harmonic distortion (THD).

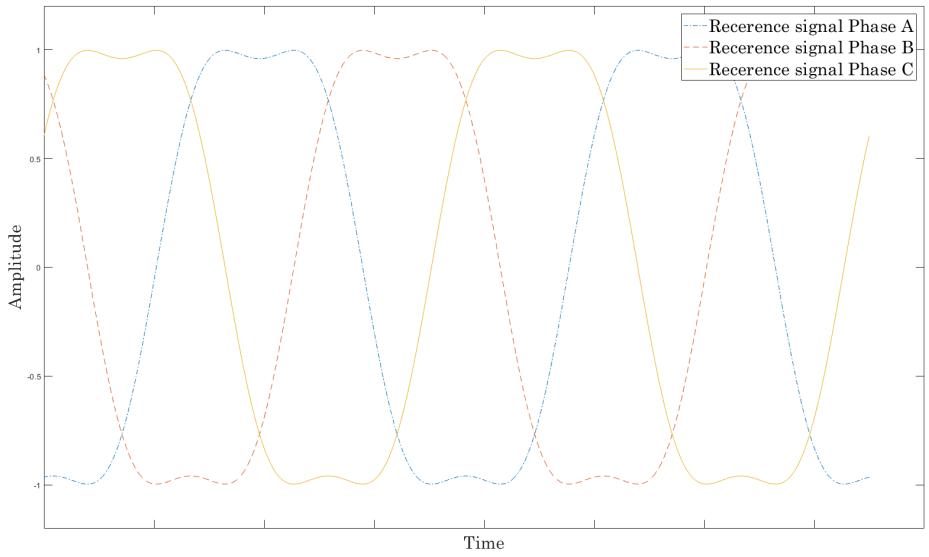

Figure 2.6: The resulting reference signal in each phase after third-order harmonic injection. The peak amplitude value of the phase signal has been flattened, while the peak value never exceeds 1, which is the maximum amplitude of the carrier signal. Thus, over-modulation is avoided to a greater extent, and the DC-link voltage is better utilized.

3

Iron Losses in Electrical Machines

As previously described in section 2.2.4, iron losses in electrical machines are a significant part of the machine's performance and efficiency and can therefore not be neglected. Unlike both mechanical and winding losses, iron losses are difficult to estimate in relation to the measured reality. The reason for this is that there is no physical method to measure and determine the iron losses directly. This chapter aims to describe in more detail what iron losses are, which factors may affect the iron losses, and what analytical methods are available to estimate the losses.

3.1 Iron Loss Classification

Iron losses occur in the magnetic parts of the machine and are created due to the altered magnetic flux in the stator and rotor. The losses can be divided into three different sections, based on their physical meaning. They will be described one by one in the following subchapters.

3.1.1 Hysteresis Losses

In ferromagnetic materials, the relationship between the magnetic flux density B and the magnetic field H is a non-linear function that depends on previous H field values. The relationship is often visualized as a curve, called hysteresis curve or hysteresis loop. An initially de-magnetized material exhibits an originating curve as H increases, the so-called virgin curve. At high values of H, the flux density will be saturated, shown in point A in figure 3.1. When the magnetic field is reduced, the flux density will follow. At some point, the field strength will reach zero, the resulting curve in point B shows that the flux density has not itself reached zero. The value of flux density remaining is called the remanence of the magnetic materials. To remove any remanence, magnetic field strength has to be reversed and increased in the opposite direction to point C. The amount of negative magnetic field strength necessary to completely remove the remanence is called coercivity. Soft magnetic materials will have a smaller coercivity field. In contrast, hard magnetic materials will have a higher, indicating that hard magnetic materials require a higher magnetic field to be de-magnetized. If the magnetic field is further increased in the negative direction to point D, the magnetic material returns to saturation in the opposite direction. The new curve will be a mirror image of the one in the positive direction, as can be seen in figure 3.1 [9].

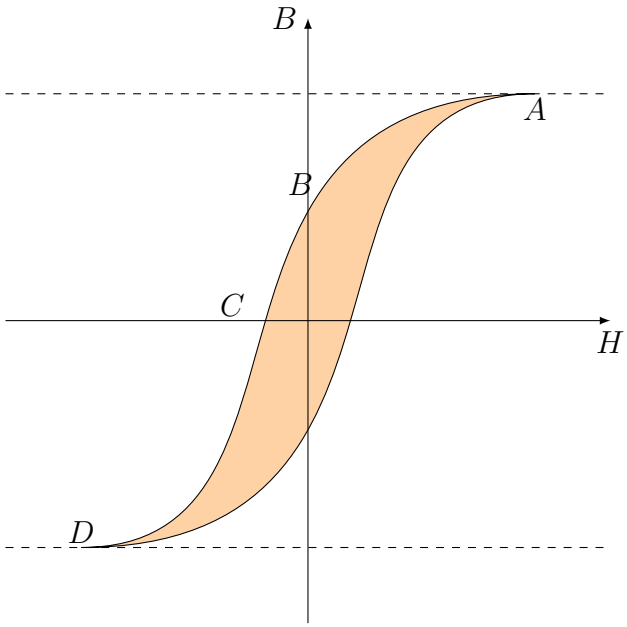

Figure 3.1: The hysteresis loop for a ferromagnetic material. The orange area represents the energy required to magnetize and demagnetize the material and is proportional to the hysteresis losses for the material.

The examined material will decide how the relationship between the magnetic flux density and the field strength looks like. The loop will be affected by the permeability of the material and its reluctance. The resulting loop area quantifies the energy required to magnetize and demagnetize the material during a cycle. The energy required to complete a cycle generates heat and is thus irreversible. This required energy will represent the hysteresis losses for a material where a larger area corresponds to more significant losses [10].

3.1.2 Eddy Currents Losses

According to Faraday's law, when an electrically conductive material is exposed to a changing magnetic field, voltages and currents will be induced. The induced current, or the eddy currents, will circulate on the surface of the material and counteract the magnetic field that caused the induced current. The magnitude of the induced currents will determine the amount of losses that eddy currents generate [11].

An effective way to minimize the eddy currents, and thus the losses due to the eddy currents, is to divide the core into thin layers along the axial length. By dividing it into several thin layers, as shown in figure 3.2, the area for each layer will be smaller. A smaller area results in a higher resistance and lower currents will be induced for the same induced voltage. The thin layers are then laminated to prevent short-circuiting between the layers. It is also common to construct the core of a material with higher resistivity. A higher resistivity increases the resistance and will reduce the eddy currents. Typically, it is possible to mix in silicon in the core to increase resistivity.

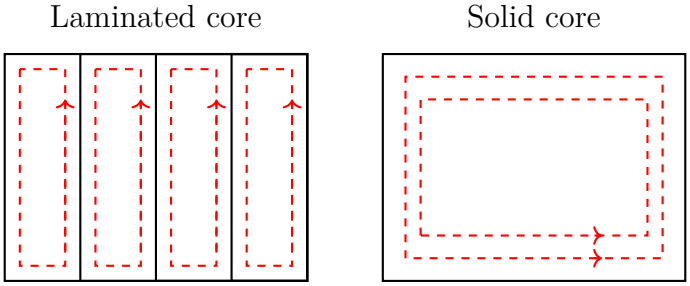

Figure 3.2: Eddy currents represented by the red loops in a solid core and a laminated core. Due to the smaller area in the laminated core, the resulting eddy currents will be lower, and thus the losses will be reduced.

3.1.3 Excess Losses

The last and the smallest contribution to iron losses in electrical machines are excess losses or anomalous losses as they also are referred to [12]. The complexity of understanding excess losses has led to the development of various theories that describe the origin of excess losses. Some theories are based on the argument that losses will occur due to the motion of the randomly distributed domain walls. Other theories describe that the occurrence of excess losses is because of the nonuniform electromagnetic flux distribution in the lamination sheets [13].

3.2 Iron Loss Modelling

The possibility to predict and investigate the iron losses is of utmost importance during the design process of electrical machines. Research within electrical machines and their losses have made it possible to model iron losses in several ways today. The models can mainly be classified into three different sets, depending on the characteristics of the model. The first, and simplest, set of models is based on the Steinmetz equation. The second group tries to separate the losses according to their physical properties. The third set of models, and the one with the highest complexity, is based on mathematical and empirical modelling of the magnetic material's hysteresis behavior. The three different sets will be described in more detail in the following sub-headings.

The equations presented for the different models will only be given in the frequency domain. Studies show that calculations in the frequency domain have been found to give up to a few percent deviations compared to calculations in time domain [14]. Furthermore, Parseval's theorem states that the sum of the frequency domain losses corresponds to the average of the time domain losses, which is important to know when comparing the two different methods [15].

3.2.1 Steinmetz Based Models

Steinmetz's approach is the basis of the first type of analytical iron loss models. The models are built on

$$p_{Fe} = \sum_{f=0}^{f_{max}} k_{SE} f^{\alpha} \hat{B}^{\beta}, \tag{3.1}$$

where p_{Fe} corresponds to the iron losses in W/kg, f the frequency of the periodic signal, and $\hat{B}$ the peak value of the flux density [16]. k_{SE}, α and β are coefficients that are obtained trough fitting to the experimental results. Initially, the Steinmetz approach was only valid for sinusoidal flux density waveforms. To make the approach more useful, a number of different modifications have been made to handle arbitrary waveforms of the flux density. The various modifications can be found in [17], where the different changes are motivated, derived, and described. Common for all variants of the Steinmetz equation is that they are relatively easy to implement to calculate the losses. The disadvantage is the coefficients' dependence on the frequency, which can give misleading results at high frequencies.

3.2.2 Separation Based models

While the models based on Steinmetz's equations model the iron losses empirically, the second group of models aims to model the losses based on their physical meaning. The first separation model was presented by Jordan [18], where the losses were separated into hysteresis losses and eddy currents losses, according to

$$p_{Fe} = p_{hyst} + p_{ed} = \sum_{f=0}^{f_{max}} k_{hyst} f \hat{B}^2 + k_{ed} f^2 \hat{B}^2 \tag{3.2}$$

where k_{hyst} and k_{ed} represents the hysteresis and eddy current coefficients. The losses due to the hysteresis, p_{hyst} are assumed to be proportional to the area of the hysteresis curve for the specific material. The losses due to the eddy currents, p_{ed} are approximated from Maxwell's equations and depend on the alternating and time-varying flux density, as well as the thickness, resistivity and the material density of the lamination sheet. The Jordan approach has been shown to produce results with lower accuracy for silicon-iron alloys. In contrast, it has been shown to reproduce experimental results very accurately for nickel-iron alloys [18]. For this reason, Bertotti improved (3.2) by introducing a third term, p_{exc}, to give a physical meaning to the excess losses [17]. The resulting equation

$$p_{Fe} = p_{hyst} + p_{ed} + p_{exc} = \sum_{f=0}^{f_{max}} k_{hyst} f \hat{B}^2 + k_{ed} f^2 \hat{B}^2 + k_{exc} f^{1.5} \hat{B}^{1.5} \tag{3.3}$$

$$p_{Fe} = k_{hyst}(f) f \hat{B}^2 + k_{ed}(f) f^2 \hat{B}^2 \tag{3.4}$$

shows the dependency of the frequency and the flux density and the separation of hysteresis, eddy current, and excess losses, respectively.
The models above assume an alternating magnetic field. In an electric machine, the magnetic field will also rotate. The phenomenon occurs mainly in the heads/tips of the teeth, but also the area between the yoke and the teethes. Thus, the rotation of the magnetic field does not occur in the majority of teeth and yoke. This rotating

magnetic field has been shown by various studies to affect iron loss [10]. Jacobs added the effect of the rotating magnetic flux to Bertotti's model (3.4), resulting in

$$p_{Fe} = \sum_{f=0}^{f_{max}} \alpha_2 f \hat{B}^2 + (k_{ed} + \alpha_4 \hat{B}^{\alpha_3}) \hat{B}^2 f^2 \tag{3.5}$$

where

$$\alpha_2 = k_{hyst}(1 + \frac{B_{min}}{B_{max}}(r-1)), \tag{3.6}$$

with r representing the rotational hysteresis factor, B_{min}, and B_{max} representing the minimum and maximum flux densities over one period. α_3 and α_4 are high order loss factors, used to fit the iron losses at high flux densities [19].

3.2.3 Mathematical Models

Provided that there are good and reliable measurements on the hysteresis curve and the material used, it is possible to make a mathematical hysteresis model with high accuracy regarding the prediction of iron losses. Two commonly used mathematical models are the classical Preisach model, as well as Jiles/Atherton model [20] [21]. Regardless of which mathematical hysteresis approach is chosen, the aim is to approximate the area of the hysteresis curve with

$$p_{Fe} = \frac{1}{T} \int_0^T H dB. \tag{3.7}$$

Some approaches have proven to be able to estimate minor loops inside the hysteresis curve, increasing the accuracy considerably [22]. All mathematical hysteresis models are rather complex and put a high demand on the number of parameters available. Due to its complexity, this report will not consider mathematical hysteresis models any further. The reader is referred to [17], [23] and [24], for further information on how they can be implemented and used.

3.3 Impact of Manufacturing

The choice of method for the estimation of iron losses will primarily affect the iron losses. Another factor that has a significant impact on iron losses is the manufacturing part. When an electric machine is produced, it undergoes a series of processes that all expose the magnetic material to various types of stress. The processes that a machine laminate typically goes through are cutting, stacking, and final assembly. During cutting, the dimensions of the laminated sheets are defined, which introduces mechanical or thermal stress depending on if punching or laser is used as a technique. The stress to which the machine is subjected will reduce the permeability of the magnetic material, increasing the hysteresis loop and thereby the losses. The relative effect from the cutting process will be more substantial for smaller and thinner sheets since the affected area in relation to the total area will be more significant. When the laminated layers are stacked together as seen in figure 3.3, it is primarily the

applied pressure that exposes the magnetic material to mechanical stress. If the sheets are welded together, local thermal stress also arises. This thermal stress can cause damage to the insulation on each sheet, which can eventually lead to short circuits and increased eddy currents. When the machine is to be placed in its housing in the final assembly process, some stress can be introduced, which negatively affects the iron losses [26].

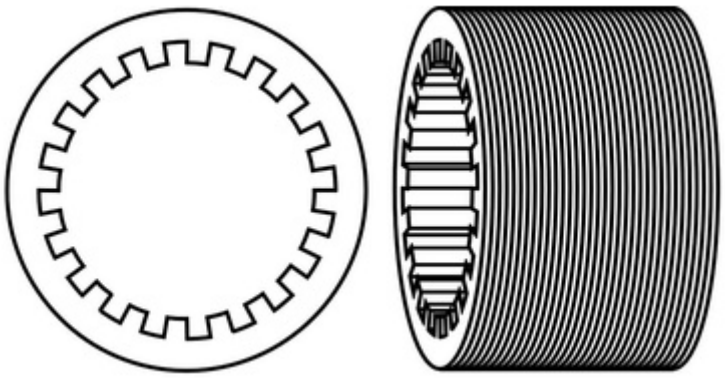

Figure 3.3: A single laminated stator sheet and several lamination sheets stacked together [25].

How much the magnetic and electrical properties are affected depends largely on the tools and processes used. The impact usually increases for thinner materials as they have less ability to cope with the externally applied stress. However, there is a way to reduce the effects of the cutting process to some extent. By subjecting the material to a heat treatment, called annealing, it is possible to reduce the impact of the external stress to which the material has been exposed to. It is worth noting that this annealing process typically only is applied to smaller machines and to machines where high efficiency is a requirement [26].

4
Modelling and Simulation Setup

The following chapters intend to explain the active choices that have been made regarding the reference machine, operating points, and iron losses. Furthermore, a essential description of how the input signal to the machine and how the modification of the iron loss model have been designed and implemented.

4.1 Machine Performance

The selected requirements of the vehicle performance and thereby the performance on the electric machine are based on the study made in [2]. In the mentioned report, three cars were conceptualized depending on performance requirements and mainly based on data found on currently top-selling BEV models. The study performed in this report will, with some modification, use the requirements of the "Highway car," which is one of the conceptualized cars in [2].

The "Highway car" is specified as a high-speed family car. More specifically, it has five seats and a top-speed that can handle highway driving in all countries (150 km/h). The main reason behind the selection is the wide speed range, which gives a broader frequency spectrum to analyze the iron losses in, and that the car is designed towards a broad area of use. In addition, the curb weight of 1700 kg is similar to a Volvo V60 ICE, which is one of the most frequently sold cars in Sweden [27]. The specified characteristics of the highway car, together with the modified ones for this project, are shown in table 4.1. As can be seen, the top speed and acceleration time were modified to higher performance. The reason behind the modification is to have a more similar performance to a combustion engine car with standard motor and similar curb weight.

From table 4.1 one can see that the car has to be able to start in 25% ascent, reach a speed of 130 km/h in 6% ascent, reach a top speed of at least 180 km/h and accelerate from 0 to 100 km/h in less than eight seconds. To transform these requirements from the car to the electric machine, the road load at different gradients was analyzed together with different constant power graphs and the tractive force to obtain the torque and power needed to fulfill the requirements. All graphs are presented in figure 4.1. The tractive force is obtained by dividing the power with the velocity of the vehicle. The net force, F_{net}, is calculated by subtracting the road load at 0% gradient from the tractive force, which results in the amount of force that can be used to accelerate the car. From figure 4.1, one can observe that 58 kW

Table 4.1: The table is showing the specified characteristics of the highway car used in this project.

Highway car characteristics	
Seats	5
Mass	1700 kg
Acceleration (0-100 km/h)	<8 s
Top speed	>180 km/h
Starting gradeability	25%
Gradeability	130 km/h at 6%
Aerodynamic drag coeff.	0.28
Area	2.3 m^2
Wheel radius	0.23 m
Rolling resistance coeff.	0.009

is needed to reach a speed of 130 km/h in 6% ascent and that 50 kW is needed to reach 180 km/h. These will be the power requirements on the machine. Further, one can also observe that there is enough net force to start in 25% ascent. This will, together with the requirement of the acceleration time between 0 to 100 km/h, set the torque requirement.

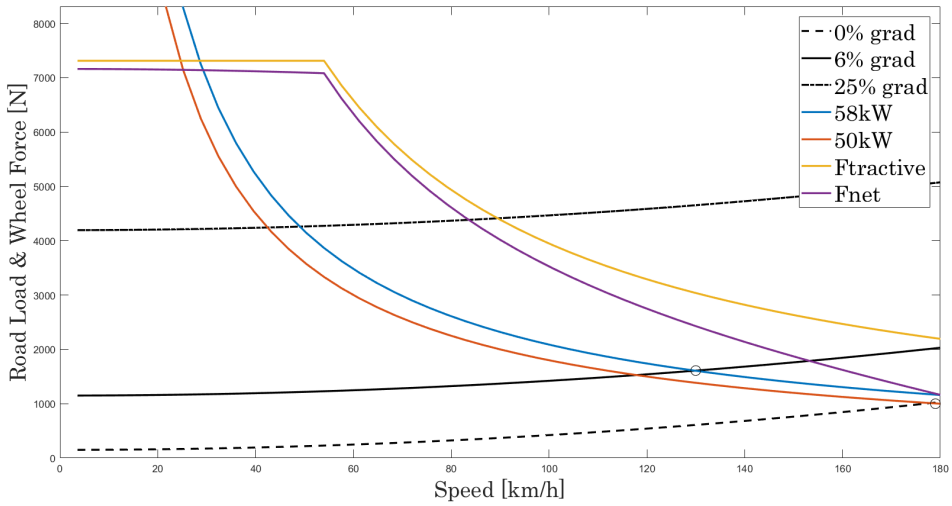

Figure 4.1: The road load at different gradients together with different constant power graphs and the tractive force are presented the figure.

After transforming the car requirements into the machine, to fulfill the requirements, the goal was to re-scale an electric machine published by the Chalmers University of Technology [29]. After some analysis, the only change needed was to change the maximum current from $300A_{rms}$ to $400A_{rms}$. The power and torque of the final machine design are together with the power requirement points presented in figure 4.2. The first three points from the left are set to reach to the acceleration requirement. The two remaining are set from the maximum speed requirements and

130km/h at 6% ascent.

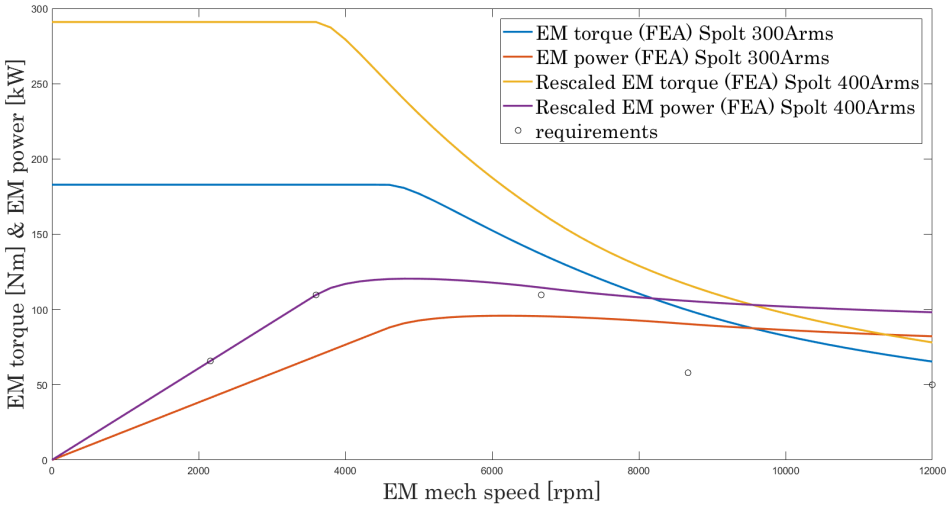

Figure 4.2: Plot of machine power and torque together with points of power requirements.

4.2 Selection of Operating Points

Using the selected reference machine and associated performance requirements, the machine's operating region was calculated using a script that computes the different operating points' circuit parameters using various combinations of id and iq, machine performance and machine parameters as input. The circuit parameters were then interpolated to find the entire operating region of the machine. The calculated circuit parameters were then used as reference values during the execution of the project.

All possible operating points for the machine should be examined to make a complete evaluation of the machine's performance when it comes to currents, voltages, and losses. It is, on the other hand, incredibly time-consuming, and for that reason, only three different operating points were selected. The selected operating points with their characteristics and their positioning in the torque curve can be seen in table 4.2 and with red markings in figure 4.3.

Table 4.2: The three different operating points and their characteristics in terms of torque, current and voltage.

Operating point	**Mech. speed** [rpm]	**Torque** [Nm]	I_d **[A]**	I_q **[A]**	U_d **[V]**	U_q **[V]**
Basespeed	4200	236.7	-441.41	353.78	-196.08	-37.28
Highest efficiency	8000	75.1	-192.7	120.41	-200.07	28.38
Maxspeed	12000	65.4	-342.01	75.97	-183.51	-84.59

The motivation behind the operating point selection was to cover as much as possible

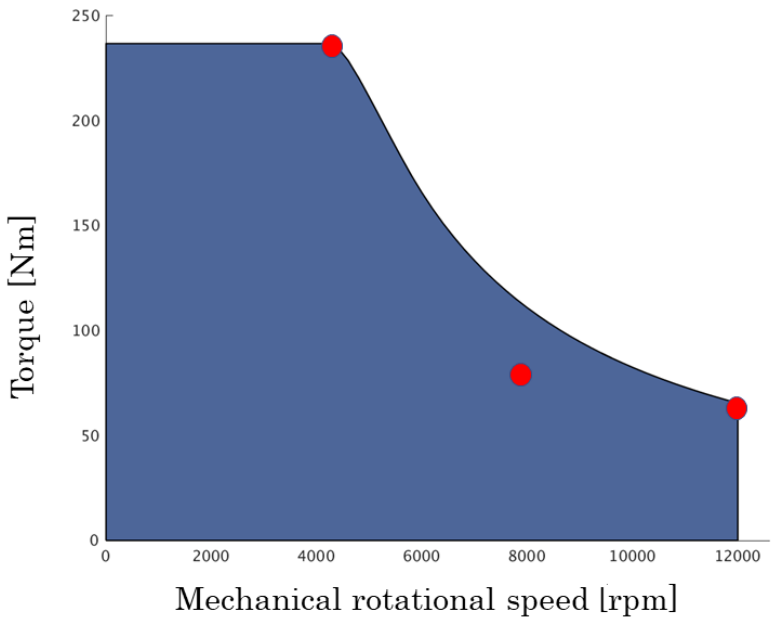

Figure 4.3: The entire operating region for the selected reference machine marked with blue colour with the three selected operating points marked with red circles.

of the operating range of the machine. Basespeed is interesting as it is the position where the currents and associated torque are at their peak. The maximum speed is of interest since the mechanical speed is the greatest, and the frequency is the highest at this point in the operating range. The last selected point is where the losses, in relation to the energy produced, are lowest. The reason for choosing this point is to see how the behavior of iron losses is when the machine is at its efficiency peak. Thus, these three points provide a rather comprehensive comparison of whether it is the current mechanical speed or other factors that could have the strongest influence on the iron losses.

4.3 Modelling the input voltages

This section will present the method of modeling the sinusoidal current and voltage feeding and the SPWM feeding. The current feeding is not the focus of this project since it is the default method and well known. It will instead be used as a reference, meaning that the aim for both the sinusoidal voltage feeding and SPWM feeding will be to regenerate the same results as the current feeding.

4.3.1 Sinusoidal feeding

To perform a sinusoidal current feeding at the selected operating points the d- and q-axis current for each operating point (presented in tabel 4.2) were used to calculate three sinusoidal time varying signals with 120 degrees shift according to

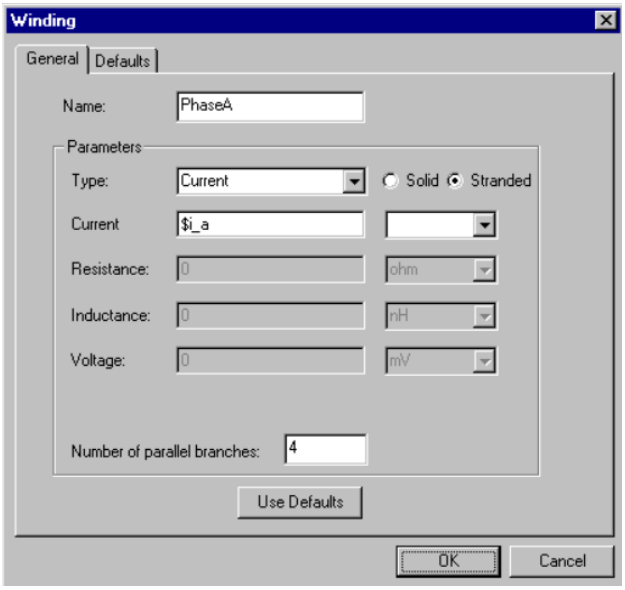

Figure 4.4: The figure displays how the winding excitation window in ANSYS Maxwell was used to perform current feeding.

$$\begin{aligned} i_a &= (\sqrt{i_d^2 + i_q^2})cos(\omega t + v) \\ i_b &= (\sqrt{i_d^2 + i_q^2})cos(\omega t - \frac{2\pi}{3} + v) \\ i_c &= (\sqrt{i_d^2 + i_q^2})cos(\omega - \frac{4\pi}{3}t + v) \end{aligned} \tag{4.1}$$

where v is an angle computed from

$$v = \arctan(\frac{i_q}{i_d}). \tag{4.2}$$

These were used to excite the machine in ANSYS Maxwell as presented in figure 4.4.

After having simulated with sinusoidal current feeding, the results were used to Park transform the resulting induced phase voltages and by that obtaining the values used for sinusoidal voltage feeding. The obtained values of the dq-voltages were used to calculate the angle and magnitude of the phase voltage in the same way as for the current. Figure 4.5 displays the set-up of a voltage excitation in ANSYS Maxwell. Compared to the current excitation, more inputs are required where initial current, stator resistance and end-winding inductance need to be specified. The initial current is set to the initial value (t=0) of each phase current. Further, a damping resistance, R_{dead}, was created as

$$R_{dead} = R_{stator} + R1_{dummy} \exp{(\frac{t}{t1_{dummy}})} + R2_{dummy} \exp{(\frac{t}{t2_{dummy}})} \tag{4.3}$$

to reduce the low frequent ripple in the torque. R_{stator} is the stator resistance, R_{dummy} are the damping resistances and t_{dummy} are the time constants. All the values are presented in table 4.3.

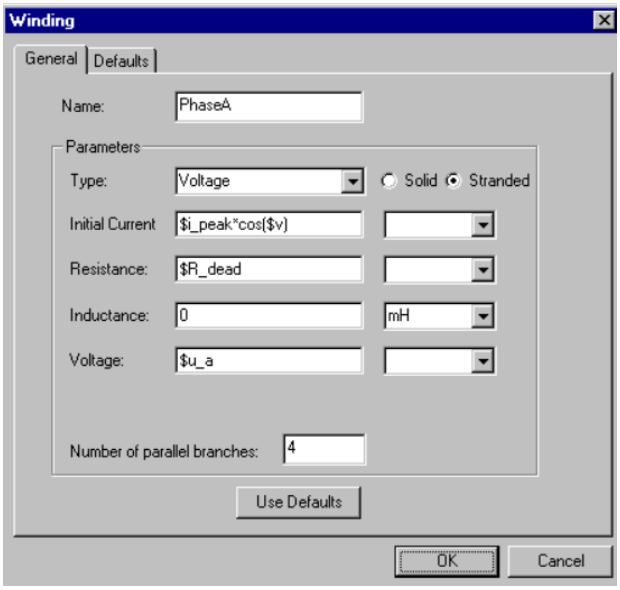

Figure 4.5: The figure displays how the winding excitation window in ANSYS Maxwell was used to perform voltage feeding.

Table 4.3: All the values of the variables for the calculation of the total resistance R_{dead}

Variable	
R_{stator}	0.01236 Ω
$R1_{dummy}$	4 Ω
$R2_{dummy}$	0.8 Ω
$t1_{dead}$	2 ms
$t2_{dead}$	4.5 ms

4.3.2 Switched feeding

To be able to feed the machine model in Ansys Maxwell with an SPWM signal, an external program was used for the generation of the SPWM signal. For this project, MATLAB was used as the inverter generator. The reference signal for each phase was created in the same way as for sinusoidal voltage feeding, where the amplitude and phase shift was calculated from the dq voltages found from the sinusoidal current feeding. The reference signals were compared with a carrier signal whose frequency was determined according to the given theory in section 2.3.1, to 10 kHz. The SPWM signal in each phase was generated by subtracting the neutral voltage from the gate voltage in each phase. Figure 4.6 shows the workflow used in MATLAB to generate the SPWM signal for phase A. In this project, the SPWM signal was modified so that the first couple of periods consisted of pure sine signals, corresponding to the reference signal. The reason for initially running the reference signal was to allow the currents, and thus the torque, to stabilize faster. The timestep for the reference signal was designed in such a way that it was larger in relation to the SPWM signal's timestep, significantly reducing the simulation times.

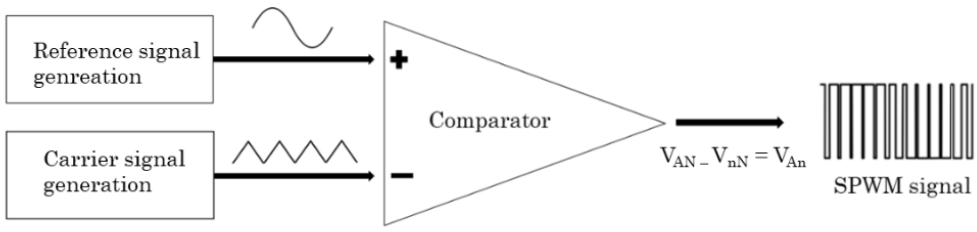

Figure 4.6: Working methodology for the generation of the SPWM signal in MATLAB

In conjunction with the creation of the SPWM signal, a new time vector was also constructed. The time vector was constructed in such a way that the time of each switch in voltage was found. This time of each switch was adjusted by a quarter of the time step backward, and a quarter of the time step forward, thus giving twice as many time steps as the number of switches. The reason for adding a time step after and before the switching event, which was shifted by a quarter of a time step, was that this would later turn out to have the lowest impact on the iron losses. Tests with both more time steps and different distances from the actual switching event were done but gave results with increased losses. In figure 4.7, the red mark shows the time step occurring at each switch, while the green dots show the time steps of the new time vector after correction. The reason for generating a time step before the switching and a time step after switching was for the definition of a square pulse wave. The procedure was repeated for all three phases to finally give a time vector containing all the switching events. Both the SPWM signal for each phase, and the new time vector were saved and imported in Maxwell. For information regarding the implementation in Maxwell, the reader is referred to Appendix A.1 .

Figure 4.7: Red marks in the left pulse representing the constructed time vector for each switch. The right pulse with the green marks represents the new time vector after correction with one-quarter of a time step resulting in a more well-defined pulse wave. The time-vector with the green markings was the one which later was used in the project.

4.4 Implementation of frequency-domain Model

In order to enable the opportunity to calculate the iron losses using a different model than ANSYS Maxwell, the time-varying magnetic flux density in every element had to be obtained. This was done using the toolkit functionality in ANSYS Maxwell. The output from the modified version of the toolkit was a matrix containing the

value of the magnetic flux density for each element in the whole time series of the simulation in a specified object of the machine.

ANSYS Maxwell uses the Bertotti model in time-domain with constant value of k_{hyst} and k_{ed} to calculate the iron losses of the machine. By using given material data, where the iron losses for a variation of flux densities at a given frequency is listed, ANSYS Maxwell performs a regression to optimize the choice of k_{hyst} and k_{ed}. This optimization can be difficult in the application of variable speed machines where there is a high variety of frequency, leading to a less performing iron loss model. Moving the calculation to frequency-domain enables the opportunity to use variable values of k_{hyst} and k_{ed} in the calculation of losses, where a optimization of the constants has been performed for each frequency using a tool in Maxwell. The different regressions are visualized in figure 4.8, where one can see that the benefit of deciding the constant for each frequency. The figure displays a comparison of Maxwells default regression to the estimated regression in this project for the frequencies $100Hz$, $1000Hz$, $5000Hz$. The estimated regression is closer to the material data in general, especially at lower frequencies. This means that for magnetic flux densities with lower harmonic content, and therefore lower frequencies, the estimated regression seems to perform better.

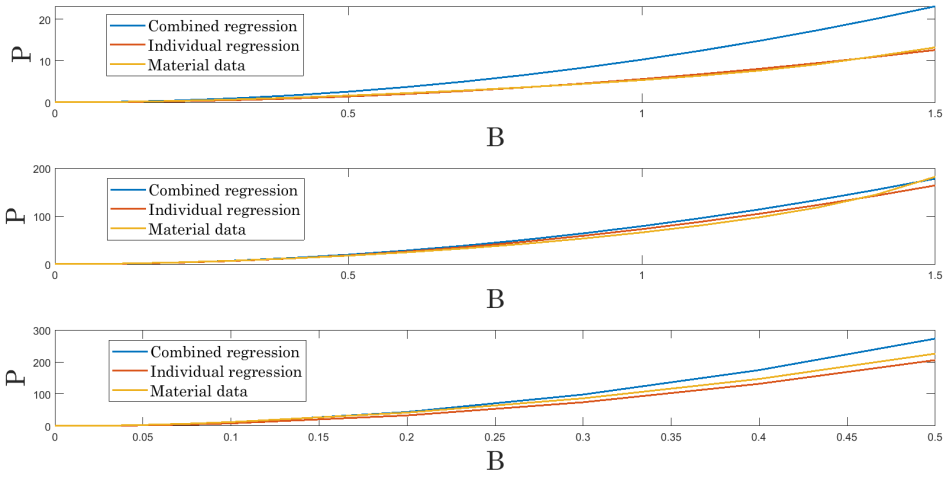

Figure 4.8: Regression curves for the Maxwell and frequency model implemented, compared to the material data for the iron used in the machine. The curves displayed are for frequencies of $100Hz$, $1000Hz$, $5000Hz$, in that order starting from above.

After deciding to perform the iron loss estimation in frequency domain, the matrices of each object from the toolkit were loaded into MatLab and used in a Fast-Fourier Transform (FFT), where the amplitudes at each frequency in the elements of the chosen object could be calculated. In the case of the SPWM signal, the signal had to be resampled as each time step was not constant, which the FFT function requires. The time vector was resampled after with different time-steps, to see how this affect the losses.

From here, the iron loss of each object in each operating point could be calculated using (3.2) presented in a previous chapter. This equation was used with constant values of k_{hyst} and k_{ed} ($k_{hyst} = 336.882$ $k_{ed} = 0.26444$) in order to verify the results since the same is used in ANSYS Maxwell but in time-domain. When the implemented calculations in MatLab were verified a tool were a variety of iron loss models could be used to perform the same calculations was obtained. The model implemented was similar to (3.2), but with varying k_{hyst} and k_{ed} for each frequency. From given material data the constants could be decided for the frequencies shown in table 4.4. In the rest of the frequencies in the span of 75-7500 Hz the constants were decided with linear interpolation. Outside the specified span the same values as in Maxwell were used.

Table 4.4: The table presents the values of k_{hyst} and k_{ed} for different frequencies.

	75 Hz	**150 Hz**	**300 Hz**	**600 Hz**	**900 Hz**	**1500 Hz**	**3000 Hz**	**7500 Hz**
k_{hyst}	115.180	131.677	118.564	127.875	210.027	200.673	583.920	432.512
k_{ed}	0.5692	0.4042	0.4698	0.4465	0.3438	0.3532	0.1616	0.1169

5

Results

In the following chapter, the different feeding techniques will be compared to each other to see how they affect the results for the iron losses. The chapter will then conclude by examining different iron loss models and how they stand against each other.

5.1 Validation of input models

In the four following sub-chapters, the results from different feeding techniques will be presented and compared to each other to see if one can reproduce the same result regardless of the feeding method. The comparison will be based on the evaluation of current, voltage, and the resulting torque. The results will be presented for all operating points in the different tables. However, the visualization of the results will only be done for the operating point at maximum speed. The reason is that the shape of the current, voltage, and torque will be the similar, regardless of the operating point.

5.1.1 Sinusoidal Current Input

Displayed in figure 5.1 are the graphs of phase currents and phase voltages with sinusoidal current feeding at the operating point called "Maxspeed". As one can observe, the harmonics are present in the voltages while the currents are perfectly sinusoidal. In figure 5.2 one can observe the machine torque over time. The torque varies around the mean value of $65.75Nm$ with a torque ripple of 9.91%.

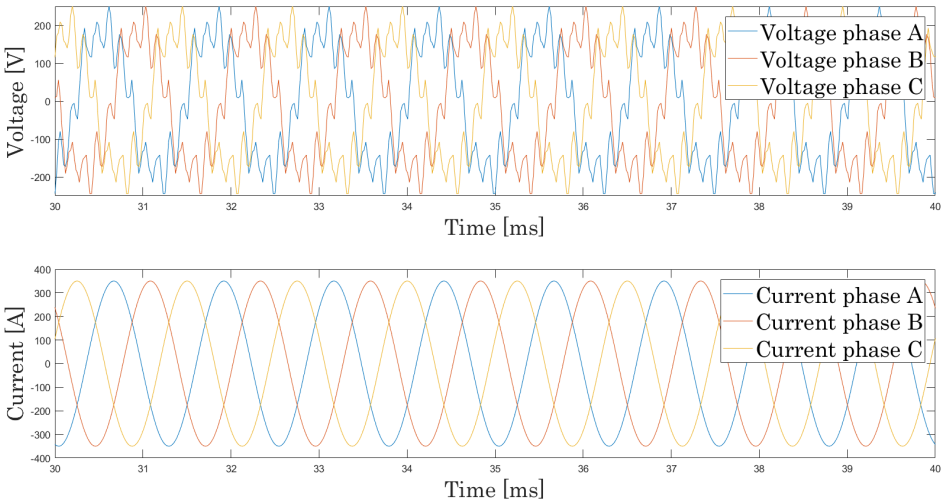

Figure 5.1: Graphs of voltage and current at the "Maxspeed" operating point.

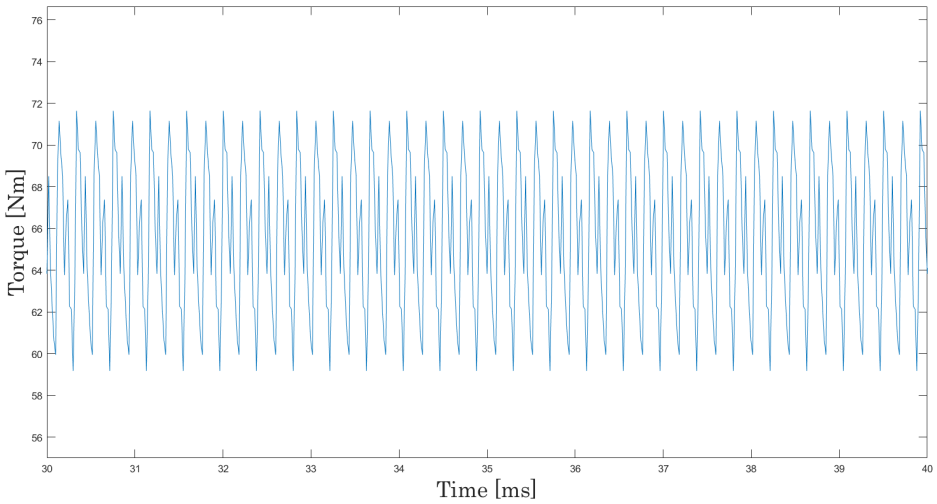

Figure 5.2: Graph of machine torque at the "Maxspeed" operating point.

In table 5.1, the results of all operating points are gathered and presented. These values are used as a reference, and the goal of the voltage feeding is to reproduce values that are as similar as possible.

Table 5.1: Sinusoidal current input characteristics for the different operating points

Operating point	I_d **[A]**	I_q **[A]**	U_d **[V]**	U_q **[V]**	**Torque [Nm]**	**Torque ripple [%]**
Basespeed	-441.41	353.78	-190.81	-38.12	236.7	8.58
Highest efficiency	-192.7	120.41	-197.4	30.5	74.11	8.03
Maxspeed	-342.01	75.97	-181.6	-82.16	65.75	9.91

5.1.2 Sinusoidal Voltage Input

Similarly, as in 5.1.1, the graphs of phase currents and phase voltages with sinusoidal voltage feeding at the operating point called "Maxspeed" are visualized in 5.3. Now the harmonics can be observed in the current while the voltage is perfectly sinusoidal. Figure 5.4 displays the torque in the same operating point, where one can observe a slightly lower mean value of 64.25 Nm and a higher ripple of 12.58 % compared with the results of the current feeding.

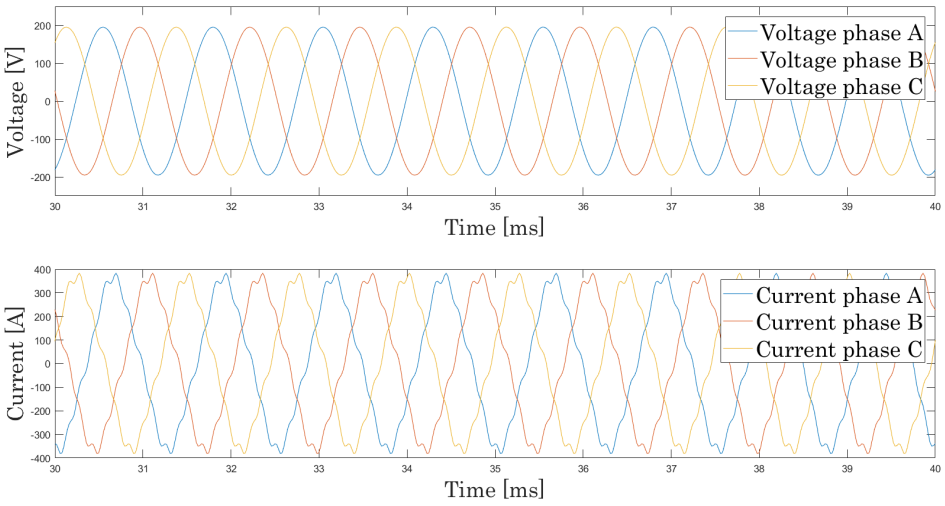

Figure 5.3: The input phase voltages and the output phase currents from the sinusoidal voltage feeding.

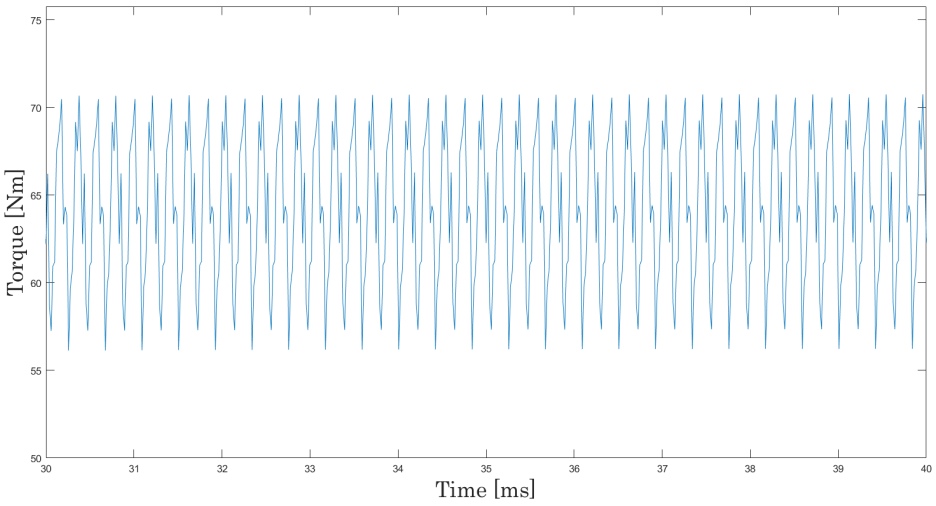

Figure 5.4: The resulting torque when feeding the machine with sinusoidal voltage signal.

In table 5.2, the results of all operating points are gathered and presented. Generally, the mean torque value is lower for voltage feeding at the chosen operating points.

The ripple is higher for the MTPA points and increases with speed for both feeding techniques.

Table 5.2: Sinusoidal voltage input characteristics for the different operating points

Operating point	I_d [A]	I_q [A]	U_d [V]	U_q [V]	Torque [Nm]	Torque ripple [%]
Basespeed	-447.9	345.99	-190.81	-38.12	235.13	7.53
Highest efficiency	-190.4	118.6	-197.4	30.5	72.5	5.45
Maxspeed	-339.73	74.6	-181.6	-82.16	64.25	12.58

5.1.3 Switched Voltage Input

In figure 5.5 and 5.6, the input voltage as well as the resulting currents and torque are visualized. As explained in the method section, the machine is initially fed with a sine wave, which after four periods, switches to a corresponding SPWM signal. By studying both figures, it can be seen that the transition to an SPWM signal does not significantly affect the results for neither current nor torque.

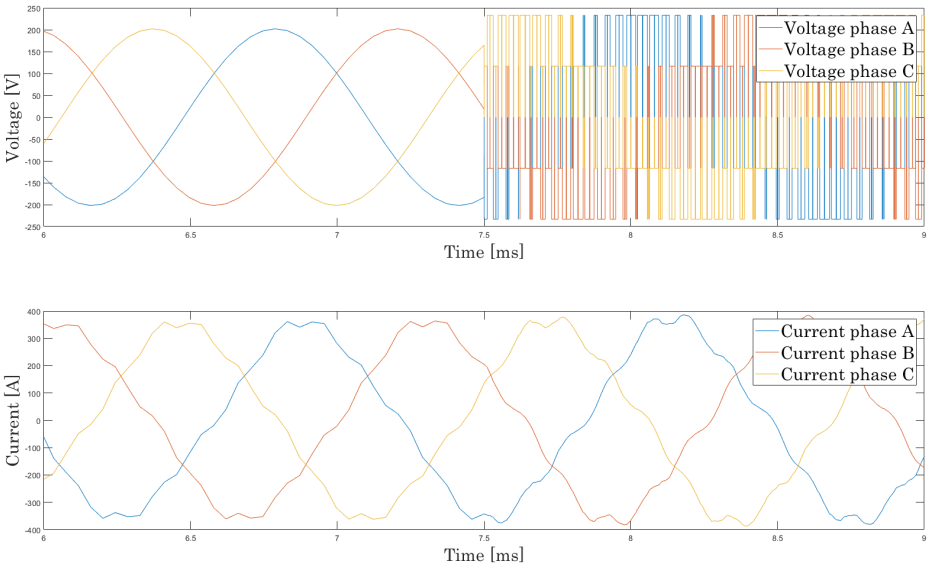

Figure 5.5: The input phase voltages and the output phase currents from the SPWM feeding. The machine is initially fed with a sinusoidal signal after 7.5 ms is changed to an SPWM signal. As in the case of sine-fed voltage, harmonics will be visible in the current. The transition to SPWM makes no visible difference in harmonics when studying the current.

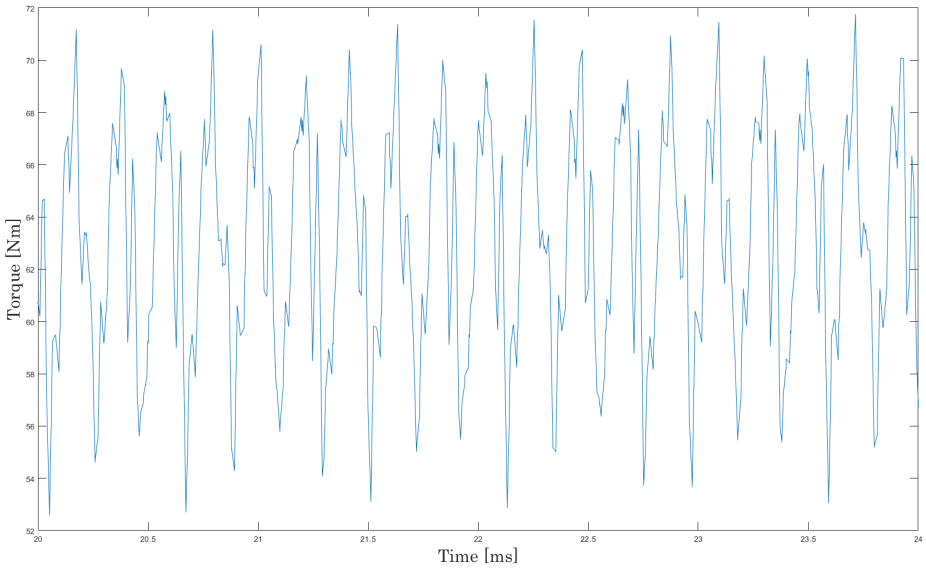

Figure 5.6: The resulting torque when feeding the machine with SPWM signal. In relation to the other two feeding techniques, SPWM will lower the torque, as well as increasing the ripple.

A closer look at the torque characteristics of the operating point at maxspeed indicates a drop in the torque compared to previous feeding techniques. In addition, the SPWM signal gives rise to an increased ripple, which amounts to just over 16 % for the operating point at maxspeed. Table 5.3 summarizes the current, voltage, torque and ripple for the various operating points. Similarly, as with both sine-fed current and sine-fed voltage, the highest ripple will be generated during the operating point at maximum speed.

Table 5.3: Switched voltage input characteristics for the different operating points

Operating point	I_d **[A]**	I_q **[A]**	U_d **[V]**	U_q **[V]**	**Torque [Nm]**	**Torque ripple [%]**
Basespeed	-438.57	345.47	-196.26	-33.74	233.58	8.83
Highest efficiency	-194.09	117.42	-199.78	31.98	72.43	8.03
Maxspeed	-343.09	70.81	-185.83	-81.22	62.32	16.5

5.1.4 Comparison of the different input models

Comparing table 5.4 with table 4.2 gives a deeper understanding of whether it is possible to reproduce the calculations of circuit parameters made during the start-up phase of the project (see section 4.2 for more information). The comparison shows that all three feeding techniques succeed in recreating the chosen operating point, with a certain margin of error. SPWM feeding is the technique that produces the absolute greatest differences, mainly in the form of lower produced torque and in the form of increased torque ripple. Furthermore, it appears that the choice of operating point could be a factor of importance. Higher speeds, like SPWM, give a larger ripple. However, no similar patterns can be seen for the other two operating

points.

Table 5.4: Comparison of the different feeding characteristics for different operating points.

Operating point	Feeding technique	I_d [A]	I_q [A]	U_d [V]	U_q [V]	Torque [N]	Torque ripple [%]
Basespeed	Sine-fed current	-441.41	353.78	-190.81	-38.12	236.7	8.58
	Sine-fed voltage	-447.9	345.99	-190.81	-38.12	235.13	7.53
	Switched voltage	-438.57	345.47	-190.81	-38.12	233.58	8.83
Highest efficiency	Sine-fed current	-192.7	120.41	-197.4	30.5	74.11	8.03
	Sine-fed voltage	-190.4	118.6	-197.4	30.5	72.5	5.45
	Switched voltage	-194.09	117.42	-197.4	30.5	72.43	8.03
Maxspeed	Sine-fed current	-342.01	75.97	-181.6	-82.16	65.75	9.91
	Sine-fed voltage	-339.73	74.6	-181.6	-82.16	64.25	12.58
	Switched voltage	-343.09	70.81	-181.6	-82.16	62.32	16.5

It should also be mentioned that the reason why the voltages are the same for one selected operating point, regardless of the feeding technique, is that the resulting voltage from the current feeding was used as input in for the voltage and SPWM feeding. Thus, it is not the voltages presented in table 4.2. This is one of the reasons why the operating point's characteristics will not be fully recreated. On the other hand, it gives a better understanding of how the different feeding techniques stand against each other, and what the effect will be of changing the feeding method.

5.2 Iron losses due to different input models

In the following chapter, the behaviour of the iron losses will be presented for the different input signals.

5.2.1 Losses with Sinusoidal Current Input

The calculated iron losses for the case of sinusoidal current feeding at the operating point called "Maxspeed" are presented in figure 5.7. The upper graph displays the total iron losses over time, while the lower visualizes the eddy and hysteresis losses in percent of total iron losses. As can be seen, the total iron losses have a mean value of around $1.6kW$ where the eddy losses are the major contributor. The total iron losses for all operating points evaluated are presented in table 5.5.

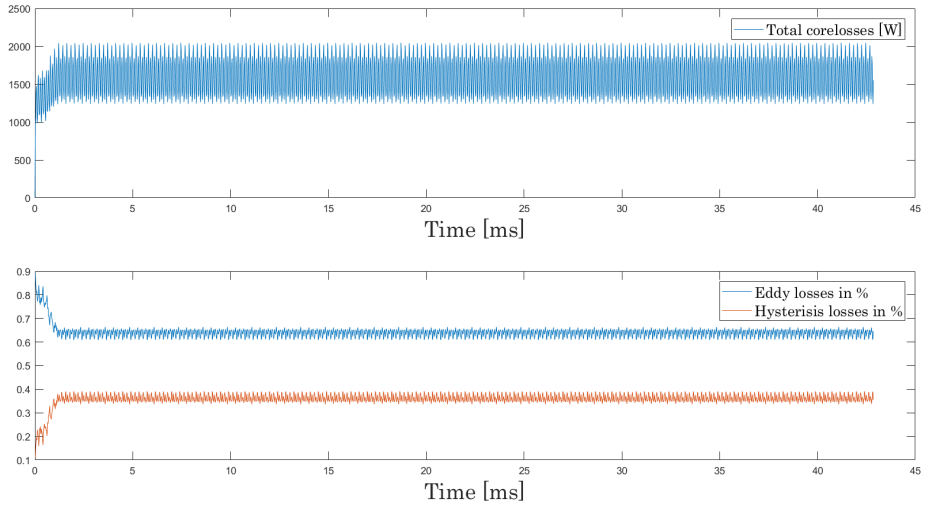

Figure 5.7: Total iron losses (upper graph) and the distribution of them in eddy and hysterisis losses (lower graph) for the operating point called "Maxspeed" in the case of current feeding.

Table 5.5: Total losses for sinusoidal current feeding at the three operating points evaluated.

Operating point	Total losses [W]
Basespeed	888,16
Efficiency	841,73
Maxspeed	1558,52

5.2.2 Losses with Sinusoidal Voltage Input

In figure 5.8, the calculated iron losses for the case of sinusoidal voltage feeding at the operating point called "Maxspeed" are presented. In like manner, the upper graph displays the total iron losses over time while the lower visualizes the eddy

and hysteresis losses in percent of total iron losses. The results are showing a mean value of around $1.5kW$ for the total losses where, as for the current feeding, the eddy losses are the major contributor. The total iron losses for all operating points evaluated are presented in table **??**.

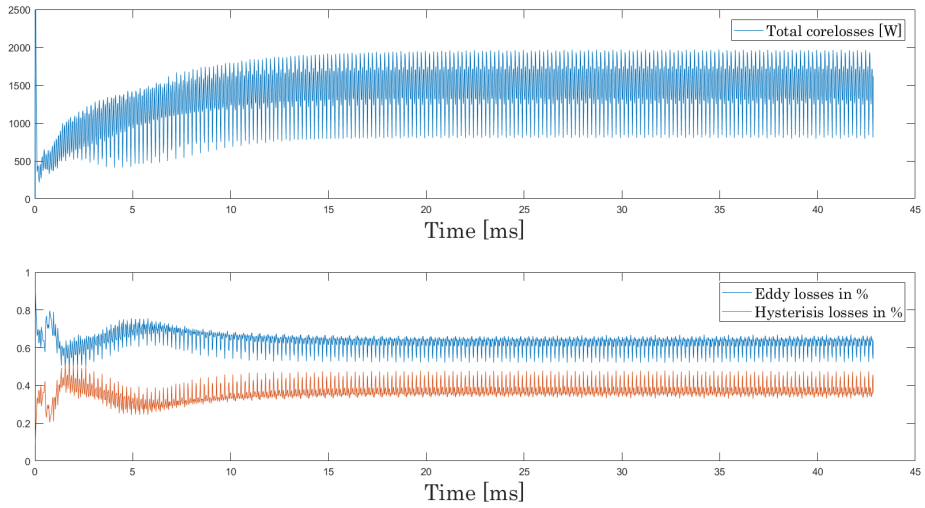

Figure 5.8: Total iron losses (upper graph) and the distribution of them in eddy and hysterisis losses (lower graph) for the operating point called "Maxspeed" in the case of voltage feeding.

Table 5.6: Total losses for sinusoidal voltage feeding at the three operating points evaluated.

Operating point	**Iron losses [W]**
Basespeed	887.75
Efficiency	887.84
Maxspeed	1526.71

5.2.3 Losses with Switched Voltage Input

The total iron losses for the three different operating points during switched voltage feeding are presented in figure 5.9. Looking at how the iron losses appear for switched voltage inputs, deviant behavior can be distinguished from the other two feeding techniques.

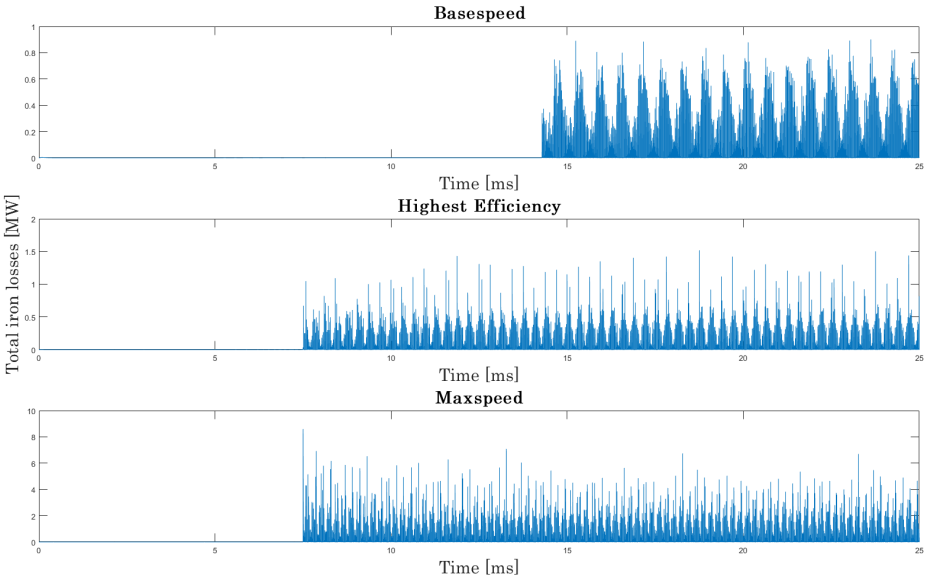

Figure 5.9: Total iron losses for the three different operating points. Increasing the speed will result in higher "spikes", which will give higher total losses.

At first, the losses look to be at a constant deficient value. When the supply switches to an SPWM signal, the losse peaks immediately rise to the MW order, which disturbs the visibility. By taking a closer look at the losses during SPWM feeding, as in the upper part of figure 5.10, it becomes clear that what appeared to be a high content of losses, is in fact "spikes" that occur at each switching event.

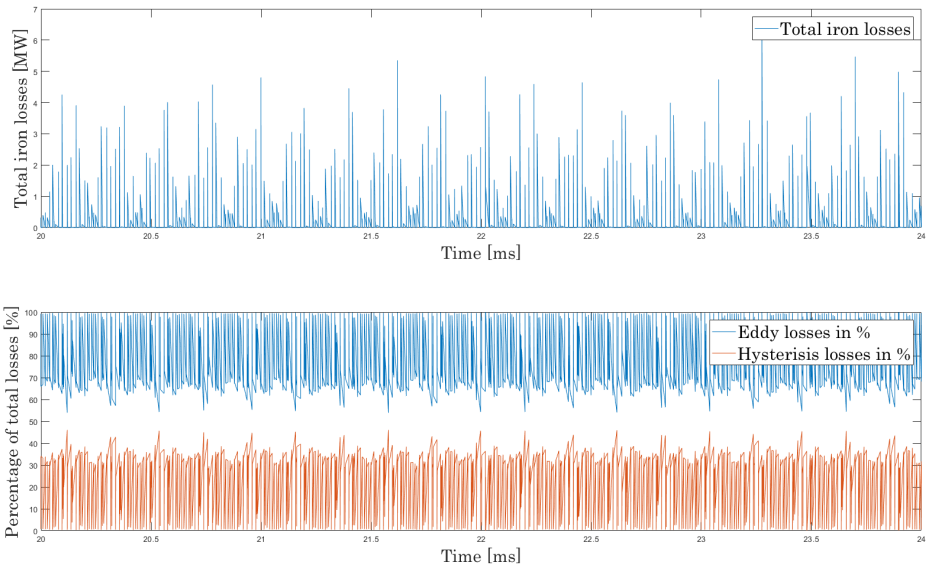

Figure 5.10: Total iron losses, and total iron losses split into hysteresis and eddy current content, for the operating point at maximum speed. The total iron losses will be dominated by eddy current losses (up to 100%) at each switching event.

These "spikes" are of MW order and will, even if they are for a short period, influence the mean value of the total iron losses. The increase in total iron losses will increase for all operating points, but it will be absolutely highest for the operating point at maximum speed. The result can be seen in table 5.7, where the losses during the initially sine signal and the descendants SPWM signal are presented. The deviation in comparison with all work points is very high and should therefore be questioned. If the results from the initial sine signal are compared with the result for the pure sine signal in table 5.6, one will see that there is a certain difference. However, the difference is considered to be small enough and in the correct order of magnitude to indicate that the importing of an external voltage signal works. The difference may be due to the fact that sampling frequency has been different in both tables.

Table 5.7: Total iron losses depending on if type of input signal. One can note that the losses due to the SPWM signal will increase with mechanical rotational speed.

Operating point	Sinusoidal signal [kW]	SPWM signal [kW]	Increase (multiple of Sine signal)
Basespeed	0.770	32.548	42.2
Highest efficiency	0.685	29.632	43.2
Maxspeed	1.327	159.177	119.9

At a closer look at how the total iron losses are distributed between eddy current and hysteresis losses (Ansys Maxwell estimates the excess losses to be equal to zero) in the lower part of figure 5.10, it can be seen that the that eddy current losses are the contributing factor to the high "spikes." For this reason, hysteresis losses will be a fraction of total iron losses during these spikes when they are, in fact, more or less constant during the simulation.

5.2.4 Comparison of losses between different input signals

Varying the feeding technology will have an impact on how the iron losses behave. The difference between sine-fed current and sine-fed voltage is relatively small. Sine-fed voltage has shown to give a variation as low as up to 5.5 %. If the machine instead is feed with an SPWM signal, losses will increase drastically, as shown in table 5.8. The big difference that arises is due to the "spikes" that occur at each switching event, which was shown in 5.2.3.

Furthermore, the choice of operating point will have a significant impact on the losses. As presented in theory, losses will increase for increasing speed, which is also seen when comparing the different operating points. The most substantial increase in losses thus becomes in the operating point at maximum speed during SPWM feeding. The reason why the losses are so similar for the operating point at basespeed and where the efficiency is highest, even though the mechanical speed is almost double for the later, only confirms that the machine is very efficient in that particular region.

Table 5.8: Total iron losses depending on the feeding technique and in comparison with sine-fed current, which is the default feeding technique in Maxwell. A value lower then one indicates that the iron losses are lower than in the case for sine-fed current.

Operating point	Feeding technique	Difference as a multiple of Sin-fed current
Basespeed	Sine-fed current	-
	Sine-fed voltage	0.956
	Switched voltage	36.665
Highest efficiency	Sine-fed current	-
	Sine-fed voltage	1.055
	Switched voltage	33.407
Maxspeed	Sine-fed current	-
	Sine-fed voltage	1.020
	Switched voltage	104.262

An operating point with the same mechanical speed, but outside the region where the efficiency is so high, would most likely result in higher iron losses. In other words, it is not only the choice of mechanical speed and feeding technology that affects iron losses. Also, the location of the operating point in the torque curve, and thus the efficiency mapping of the machine will affect the result.

5.3 Verification of frequency-domain calculation

A first step in modifying the loss calculation was to compare Ansys Maxwell's calculations with the calculations made after extracting the time-varying magnetic flux. Bertotti's iron loss model in (3.4) was used for the calculation, where the excess losses were set to zero, to recreate the calculations in Maxwell. The result in table 5.9 shows the difference in percentage between the calculations in Maxwell and the calculations made with the Bertotti equation in frequency domain. The table shows that by extracting the time-varying magnetic flux in all elements, it is possible to recreate the calculations that Maxwell does for sine-fed current and sine-fed voltage feeding with a relatively small error.

Table 5.9: The difference in percentage between Maxwell's calculations of the total losses for the machine and the total losses calculated in frequency domain using the implemented toolkit. A negative percentage corresponds to the calculated losses being lower than the calculation performed by Maxwell.

	Current feeding	Voltage feeding	SPWM Feeding
Basespeed	- 3.45 %	- 7.21 %	-
Highest efficency	- 0.91 %	- 8.76 %	-
Maxspeed	0.72 %	4.54 %	-

The difference in percentage is smallest for sine-fed current, but where sine-fed voltage is not far off. Furthermore, the calculation always gives a lower estimate for the two operating points with a lower mechanical speed while providing a small overestimation of the operating point at maximum speed. For loss calculations,

when the machine is fed with an SPWM signal, the result has not been included. The reason for this is the difficulties in transforming the signal in time domain to frequency domain. The simulation of the losses generated by an SPWM signal has been found to be very sensitive to the selection of sampling frequency, which was not experienced for the other two feeding techniques. In figure 5.11 it is possible to see how the total iron losses are affected by the choice of sampling frequency, where increased sampling frequency results in increasingly higher losses. Already at sampling frequencies higher than 40 MHz, the calculated losses in the frequency domain are higher than Maxwell calculates. One possible explanation for this behavior is how the SPWM signal is resampled, as explained in 4.4. In other words, a higher sampling frequency, or shorter time-step, results in larger spikes of iron losses than Maxwell estimates the spikes, which results in higher losses.

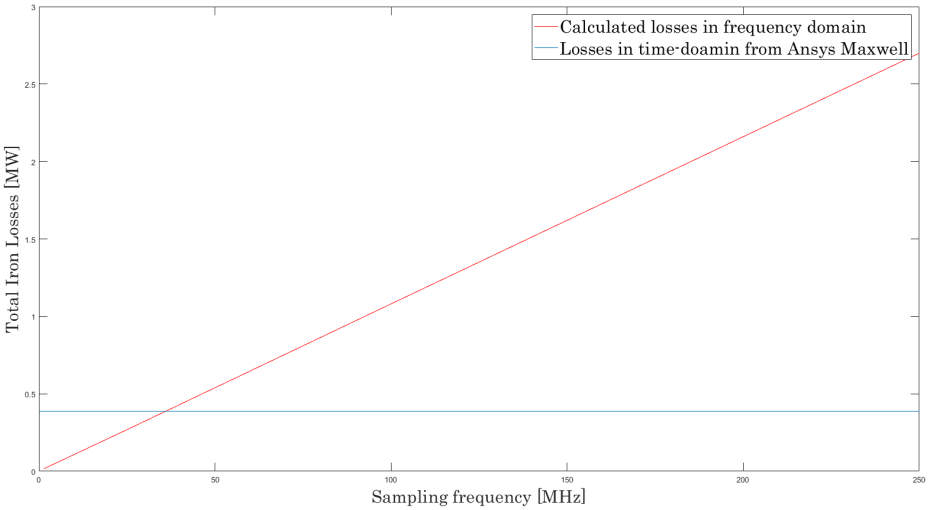

Figure 5.11: The behavior of total iron losses for different sampling frequencies.

5.4 Loss Calculation With Modified Iron Loss Model

In this section the calculated losses with the modified iron loss model in frequency domain are presented where the values of k_{hyst} and k_{ed} were varied as in table 4.4. Table 5.10 displays the results in all operating point for the three different feeding techniques. A comparison to the frequency model with constant k_{hyst} and k_{ed} is made as well, where the difference is presented in percentage. As can be noticed, the modified model has lower losses in all the points compared. Since the default frequency model has lower losses compared to Maxwell's model, the comparison to Maxwell's results to this modified frequency model will result in even higher differences. This was expected considering that the regression curves in figure 4.8 shows that Maxwell overestimates the losses especially at lower frequencies where the fundamental frequency will be at these machine velocities.

Table 5.10: Total iron losses with modified iron loss model depending on the feeding technique and in comparison with the results from the default Maxwell model. Negative percentage implicates that the results from the modified model are lower.

Operating point	**Feeding technique**	**Total iron losses [W]**	**Diff in % vs frequency domain model with constant k_{hyst} and k_{ed}.**
Basespeed	Sine-fed current	615	-33.9
	Sine-fed voltage	614	-34.0
	Switched voltage	-	
Highest efficiency	Sine-fed current	679	-18.6
	Sine-fed voltage	675	-17.4
	Switched voltage	-	
Maxspeed	Sine-fed current	1229	-18.4
	Sine-fed voltage	1172	-17.7
	Switched voltage	-	

6
Discussion

Firstly, and probably foremost, the results presented should be validated to experimental data from the same machine used in the simulations. By comparing with experimental data, it is possible to compare how different results stands against each other with greater certainty. This is particularly important when evaluating different iron loss models.

6.1 Selection off operating points

One central comparison during the project has been to compare the iron losses based on feeding technology and the type of iron loss model. This has been done by comparing the results for three different operating points for the machine. The operating points were initially chosen in an attempt to cover different areas of the machine's working environment. However, it has been found that that the analysis would had benefited from evaluating more points. Given that only three points were evaluated, it has been challenging to find any clear trends as to whether the feeding technology or selection of the iron loss model has had any impact on the simulated results. In the case where it has been possible to discern clear trends, it has not been possible to confirm whether the patterns can be confirmed with certainty.

Comparing all operating points for the machine would be the optimal solution, and would most likely provide a better overview of how specific parameters affect the iron losses. It would, however, be incredibly time-consuming and resource-consuming. It is, therefore, possible to discuss whether the choice of operating points fulfilled its function, or whether other positions should have been chosen. In this project, the operating points in the torque curve were chosen where the machines in vehicle applications are rarely exposed to any great extent. On the other hand, it allowed a comparison of how the losses appear for maximum mechanical speed, and where the currents are at their peak. The operating point's location could be located where the machine is often operating, preferably at very low speeds corresponding to the start-stop scenario. Another scenario is to place an operating point along with the car's road load, to investigate how the iron losses appear at a load that a vehicle is commonly exposed to. One final scenario, and possibly the one that would give the best result for an evaluation similar to the one in this report, could be to set a fixed torque and only vary the mechanical speed by a few hundred rpm. Preferably, these operating points would be located in an area where the machine's efficiency is constant. This would allow a better comparison of how the losses are affected by

speed and different feeding techniques. The iron losses are thus still not neglectable, which confirms that it is essential to study and consider the iron losses during machine design.

6.2 Effect off feeding technique

The choice of feeding technique has been found to have a significant impact on the behavior of iron losses. The difference between sine-fed voltage and current has been found to give minimal differences; in some cases, the sine-fed voltage has caused slightly lower losses. However, switched voltage has shown to cause significantly higher losses. Regardless of operating point, switched voltage causes losses in megawatts order. This can be compared to losses in kilowatt sizes for the other feeding techniques or the total power of the machine which is around 100 kW. From these comparisons it is obvious that the iron losses shown in the modelling of switched voltage feeding are unrealistic. The fact that these spikes also indicate trends, where they increase in magnitude, with increasing speeds, makes this even more problematic. The large increase in losses could be due to the fact that for both sine-fed current and voltage, Ansys Maxwell itself generates the input signal, while for switched voltage feeding, the externally generated input signal is imported.

The difference between feeding techniques is not entirely unexpected. Previous studies at the Chalmers University of Technology, among others, show that iron losses can increase by more than 100 % for speeds at 3500 rpm and relatively low torque values, when feeding technology is switched from sine-fed current to SPWM [28]. Simulations in this project also show that a change in feeding technology will affect the results, and that it is the SPWM signal that will give highest contribution to iron losses. However, the fact remains that the losses increase to unreasonably high levels when the machine is fed with an SPWM signal if the results are compared with the above given source.The losses for the operating point at the highest mechanical speed may be considered too high and deviating. Simulations for this operating point should therefore be investigated, where primarily the definition of the new time vector should be investigated. In the project, as presented in section 4.3.2, one point in the time vector was generated just before the switching event, and another just after the switching event. Some simple simulations were done, where the number of points and the time from the switching event were varied. The results from this simulations, which are those used according to section 4.3.2, gave the lowest losses. In other words, the losses appear to be strongly dependent on how the time vectors are generated. Besides this, it should be said that it is not excluded that other constellations of the new time vector could give rise to less deviating losses.

By generating the feeding signal through the externally the right operating point was obtained, while one could observe that the losses of the sine-fed voltage did not reproduce similar results. As mentioned, the reason behind this deviation in losses is unknown and has to be further investigated in order to obtain more reliable results for the SPWM feeding. Changing the time-vector or the averaging of the

signal could be possible solutions.

6.3 Verification in frequency domain

The importance of comparing simulations with experimental data is crucial for the verification of the modified frequency model and the estimated regressions to material data. With this data one could confidently state which model performs best. From this, more iron loss models could easily be evaluated from the tool created by extracting the magnetic flux density in all elements. Including rotational losses is a recommended approach because of the machine's rotational flux.

Another recommended improvement would be to implement a different tuning of the values of k_{hyst} and k_{ed} for each frequency. The tool used to extract these constants is not optimized for this usage, even though it uses the material data and has performed a good regression. Writing a new script for this application could probably tune in the constants even better, which would result in a even better regression giving more accurate iron losses. In addition to this the material data available in this project is given in a specific frequency span which limits the possibility to tune the constants k_{hyst} and k_{ed} outside this span. Finding material data for a broader frequency span could generate some improvement to the iron loss calculations.

6.4 Ethical and Environmental aspects

The ethical and environmental discussion around this projects is centered in the usage of a machine that is magnetized with permanent magnets. The rare earth materials cobalt and neodymium which are used in magnets are in majority mined in China and Congo where both child-labour and horrible working conditions are a reality. Improving the iron loss modelling could promote the usage of electric machines further and imply a higher demand of rare earth materials. This would probably lead to more mines implying for instance more child-labour. The ongoing electrification is facing these problems and the risks will hopefully be at least reduced by companies taking responsibility and making sure that their supply-chain is fair traded. On individual level one can contribute by choosing those car-manufacturers that are showing awareness of these problems. The higher energy density of PMSM compared to for example an induction machine (IM) which has the benefit of not using magnets, will on the other hand reduce the usage of copper compared to the IM. The mining of copper is also dangerous and done in countries with bad working conditions.

The increased mines will affect the environment negatively because landscapes will be destroyed. This can affect people living nearby and in worst case forcing them to move. By destroying landscapes the habitat of some animals would probably be lost, which could end up threatening the biodiversity in the area. At the same time, this project attempts to contribute to the electrification of today's transport and reduce the greenhouse gases which are proven to threaten our climate.

7
Conclusion

Three different feeding techniques have successfully been implemented in Ansys Maxwell to compare the behavior of iron losses based on the feeding technology.

The result for the comparison of varying feeding techniques in different operating points shows that the difference between sine-fed current and sine-fed voltage is minimal. SPWM feeding, on the other hand, gives rise to an increase in iron losses. The sharp increase in losses is due to the fact that spikes occur in megawatt orders at every switching event. Furthermore, it can be stated that increasing mechanical speed results in increased losses. In addition to mechanical speed and feed technology, the choice of operating point has a contributing factor to the size of the iron losses.

Finally, the existing iron loss model in Ansys Maxwell was modified by varying the parameters k_{hyst} and k_{ed}, which reduced the losses up to 34 %. The results of the modification are considered to be closer to reality, given that the parameters are better parametrized to material data from manufacturers than before. Only when the results of the simulations can be compared to the experimental data can it be said with certainty whether the results are closer to reality or not. By providing more accurate material data, the modification could be further developed.

Bibliography

[1] A. Krings, "Iron Losses in Electrical Machines — Inuence of Material Properties, Manufacturing Processes, and Inverter Operation," Ph.D dissertation, pp. 1-8, KTH Royal Institute of Technology, Stockholm, 2014. Accessed on: Jan 22, 2020. [Online]. Available: Available: ISBN: 978-91-7595-099-0

[2] E.A.Grunditz, "Design and Assessment of Battery Electric Vehicle Powertrain, with Respect to Performance,Energy Consumption and Electric Motor Thermal Capability, thesis for the degree of doctor of philosophy, Chalmers University of Technology, Gothenburg, 2016. Accessed on: Feb 17, 2020. [Online]. Available:http://www.chalmers.se/SiteCollectionDocuments/Energi

[3] A. Krings, "Iron Losses in Electrical Machines — Inuence of Material Properties, Manufacturing Processes, and Inverter Operation," Ph.D dissertation, pp. 9-17, KTH Royal Institute of Technology, Stockholm, 2014. Accessed on: Jan 22, 2020. [Online]. Available: ISBN: 978-91-7595-099-0

[4] C. V. Suru ; C. A. Patrascu, "The Synchronous Fundamental dq Frame Theory Application for the Active Filtering", *2014 International Conference on Applied and Theoretical Electricity (ICATE)* Accessed on Feb. 2, 2020. [Online]. Available: doi: 10.1109/ICATE.2014.6972654

[5] T. Bariša, D. Sumina and M. Kutija, "Comparison of maximum torque per ampere and loss minimization control for the interior permanent magnet synchronous generator," 2015 International Conference on Electrical Drives and Power Electronics (EDPE), Tatranska Lomnica, 2015, pp. 497-502. DOI: 10.1109/EDPE.2015.7325344

[6] B. Van Der Pol, "Frequency Modulation," *Proceedings of the Institute of Radio Engineers*, vol. 18, no. 7, pp. 1194-1205. Accessed on: Mar 29, 2020. [Online]. DOI: 10.1109/JRPROC.1930.222124.

[7] K. T. Chau, Electrical Vehicle Machines and Drives. Hong Kong. John Wiley Sons Singapore Pte. Ltd., 2015, pp. 50. Accessed on: Apr. 2, 2020. [Online]. DOI: 10.1007/978-94-015-9387-8

[8] I. Colak, R. Bayindir and E. Kabalci, "A modified harmonic mitigation analysis using Third Harmonic Injection PWM in a multilevel inverter control," *Proceedings of 14th International Power Electronics and Motion Control Conference EPE-PEMC 2010*, Ohrid, 2010, pp. T2-215-T2-220. Accessed on: Mar 29, 2020. [Online]. DOI: 10.1109/EPEPEMC.2010.5606607.

[9] V. Malo Machado and A. Lopes Ribeiro, "Eddy current and hysteresis losses in ferromagnetic media," *IEEE Transactions on Magnetics*, vol. 34, no. 4, pp. 1267-1269, July 1998, . Accessed on: Mar 29, 2020. [Online]. DOI: 10.1109/20.706517.

[10] A. Krings, "Iron Losses in Electrical Machines — Inuence of Material Properties, Manufacturing Processes, and Inverter Operation," Ph.D dissertation, pp. 25-36, KTH Royal Institute of Technology, Stockholm, 2014. Accessed on: Jan 22, 2020. [Online]. Available: ISBN: 978-91-7595-099-0

[11] P. D. Agarwal, "Eddy-current losses in solid and laminated iron," *Transactions of the American Institute of Electrical Engineers, Part I: Communication and Electronics*, vol. 78, no. 2, pp. 169-181. Accessed on: Mar 29, 2020. [Online]. DOI: 10.1109/TCE.1959.6372977.

[12] L. Jingsong, Y. Qingxin, L. Yongjian and Z. Changgeng, "Anomalous Loss Modeling and Validation of Magnetic Materials in Electrical Engineering," *IEEE Transactions on Applied Superconductivity*, 2016. Accessed on Feb. 27, 2020. [Online]. DOI: 10.1109/TASC.2016.2526786.

[13] Y. Zhang, M. Cheng and P. Pillay, "Magnetic Characteristics and Excess Eddy Current Losses," *2009 IEEE Industry Applications Society Annual Meeting*, 2009, pp. 1-5. Accessed on Mar. 2, 2020. [Online]. : DOI: 10.1109/IAS.2009.5324814

[14] D. Kowal, P. Sergeant, L. Dupré and L. Vandenbossche, "Comparison of Iron Loss Models for Electrical Machines With Different Frequency Domain and Time Domain Methods for Excess Loss Prediction," in IEEE Transactions on Magnetics, vol. 51, no. 1, pp. 1-10, Jan. 2015, Art no. 6300110, Accessed on May. 20, 2020. [Online]. DOI: 10.1109/TMAG.2014.2338836.

[15] S. S. Kelkar, L. L. Grigsby and J. Langsner, "An Extension of Parsevals Theorem and Its Use in Calculating Transient Energy in the Frequency Domain," *IEEE Transactions on Industrial Electronics*, vol. IE-30, no. 1, pp. 42-45, Feb. 1983. Accessed on May. 20, 2020. [Online]. DOI:10.1109/TIE.1983.356702.

[16] C.P, Steinmetz, "On the law of hysteresis", *Proceedings of the IEEE*, vol. 72, no. 2, pp. 196-221, 1984. Accessed on Feb. 2, 2020. [Online]. Available: doi:10.1109/PROC.1984.12842

[17] D. Kowal, P. Sergeant, "Comparision of Iron Loss Models for Electrical Machines With Different Frequency Domain", *IEEE Transactions on magnets*, vol. 51, no. 1, pp. 1-10, 2015. Accessed on Jan. 30, 2020. [Online]. Available: DOI: 10.1109/TMAG.2014.2338836

[18] J. Juergens, B. Ponick, O. Winter and A. Fricassè, "Influences of iron loss coefficients estimation on the prediction of iron losses for variable speed motors," *2015 IEEE International Electric Machines Drives Conference (IEMDC)*, Coeur d'Alene, ID, 2015, pp. 1254-1259, Accessed on Jan. 30, 2020. [Online]. Available: DOI: 10.1109/IEMDC.2015.7409222.

[19] L. Vandenbossche, S. Jacobs, "Improved iron loss modelling approach for advanced electrical steels operating at high frequencies and high inductions in automotive machines," *2012 2nd International Electric Drives Production Conference (EDPC)*, Nuremberg, 2012, pp. 1-8. Accessed on Feb. 12, 2020. [Online]. Available: DOI: 10.1109/EDPC.2012.6425108

[20] A. R. P. J. Vijn, O. Baas and E. Lepelaars, "Parameter Estimation for the Jiles–Atherton Model in Weak Fields," *IEEE Transactions on Magnetics*, vol. 56, no. 4, pp. 1-10, April 2020, Art no. 7300510, Accessed on May. 20, 2020. [Online]. DOI: 10.1109/TMAG.2020.2971435.

[21] Y. Bernard, E. Mendes and F. Bouillault, "Dynamic hysteresis modeling based on Preisach model," in IEEE Transactions on Magnetics, vol. 38, no. 2, pp. 885-888, March 2002, Accessed on May. 20, 2020. [Online]. DOI: 10.1109/20.996228.

[22] T. Taitoda, Y. Takahashi and K. Fujiwara, "Iron Loss Estimation Method for a General Hysteresis Loop With Minor Loops," *IEEE Transactions on Magnetics*, vol. 51, no. 11, pp. 1-4, Nov. 2015, Art no. 8112304, Accessed on May. 20, 2020. [Online]. DOI: 10.1109/TMAG.2015.2445930.

[23] A. Krings, J. Soulard, "Overview and Comparison of Iron Loss Models for Electrical Machines", *Journal of Electrical Engineering*, vol. 10, pp. 162-169, 2010. Accessed on Feb. 11, 2020. [Online]. Available: https://www.researchgate.net/publication/228490936

[24] G. Paltanea, V. Paltanea, G. Horia, "Mathematical approach of hysteresis phenomenon and energy losses in non-oriented silicon iron sheets," *UPB Scientific Bulletin, Series A: Applied Mathematics and Physics.*, 2015, vol. 77, pp. 241-252. Accessed on Feb. 12, 2020. [Online]. Available: DOI: 10.1109/EDPC.2012.6425108

[25] T. Tudorache, M. Mircea., "Design Solutions for Reducing the Cogging Torque of PMSM," *Advances in Electrical and Computer Engineering*, 2013, Vol. 13 pp. 61. Accessed on Mar. 2, 2020. [Online]. DOI: 10.4316/aece.2013.03010.

[26] M. Florence, J. Soulard, "PMSMs with Non-Overlapping Concentrated Windings: Design Guidelines and Model References," *Ecological vehicles - Renewable energies , Monaco* , 2009. Accessed on Feb. 13, 2020. [Online]. Available: https://www.researchgate.net/publication/228352876

[27] BILsweden, Nybilsregistrering, vol. number, Sweden, Publisher:BILsweden.se , 2020. Accessed on: April. 1, 2020. [Online]. Available: http://libraryguides.vu.edu.au/c.php?g=403938p=6008962

[28] A. Andersson, "Electrical Machine Control forEnergy Efficient Electric Drives Systems ," Ph.D dissertation, Chalmers University of Technology, Göteborg, 2018. Accessed on: June 3, 2020. [Online]. Available: https://research.chalmers.se/publication/504662/file/504662Fulltext.pdf

[29] E. Jansson, T. Thiringer and E. Grunditz, "Convergence of Core Losses in a Permanent Magnet Machine, as Function of Mesh Density Distribution, a Case-Study Using Finite-Element Analysis," *IEEE Transactions on Energy Conversion*. Accessed on Jun. 10, 2020. [Online] DOI: 10.1109/TEC.2020.2982265. (**??**)

[30] A. Krings, "Iron Losses in Electrical Machines — Inuence of Material Properties, Manufacturing Processes, and Inverter Operation," Ph.D dissertation, pp. 19-23, KTH Royal Institute of Technology, Stockholm, 2014. Accessed on: Jan 22, 2020. [Online]. Available: Available: ISBN: 978-91-7595-099-0

[31] A. Krings, "Iron Losses in Electrical Machines — Inuence of Material Properties, Manufacturing Processes, and Inverter Operation," Ph.D dissertation, pp. 37-45, KTH Royal Institute of Technology, Stockholm, 2014. Accessed on: Jan 22, 2020. [Online]. Available: Available: ISBN: 978-91-7595-099-0

[32] A. Krings, "Iron Losses in Electrical Machines — Inuence of Material Properties, Manufacturing Processes, and Inverter Operation," Ph.D dissertation, pp. 87-

102, KTH Royal Institute of Technology, Stockholm, 2014. Accessed on: Jan 22, 2020. [Online]. Available: ISBN: 978-91-7595-099-0

A

Appendix

A.1 Importing tab-files in Maxwell

Both the SPWM signal for each phase, and the new time vector were saved as tab-files, a format supported by Maxwell. The files were imported to Maxwell and called with the *pwlx(y, time)* command. The pwlx function interpolates tab-file y along the x-axis, which henceforth will be the time vector. It should be said that the tab-files must be imported under the Design level (*Menu item > Maxwell 2D/3D > Design Data set > Import*), and not in the Project level (*Menu item > Project > Data set > Import*). If they are imported under Project level, the pwlx command cannot access the tab-files. The tab files are called in two places, both in Winding setup and in Analysis setup. Figure A.1 and A.2 shows how the command was used, as well as the setting options for each tab.

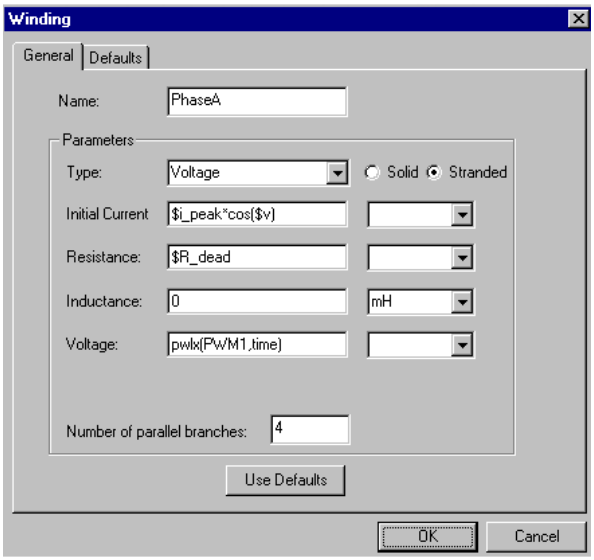

Figure A.1: Available settings for the Winding setup. The settings are the same as they are described for sinusoidal voltage, the slight difference is that in the Voltage window the tab-file PWM1 is accessed with the pwlx command. In this case, PWM1 corresponds to the generated SPWM signal for phase A.

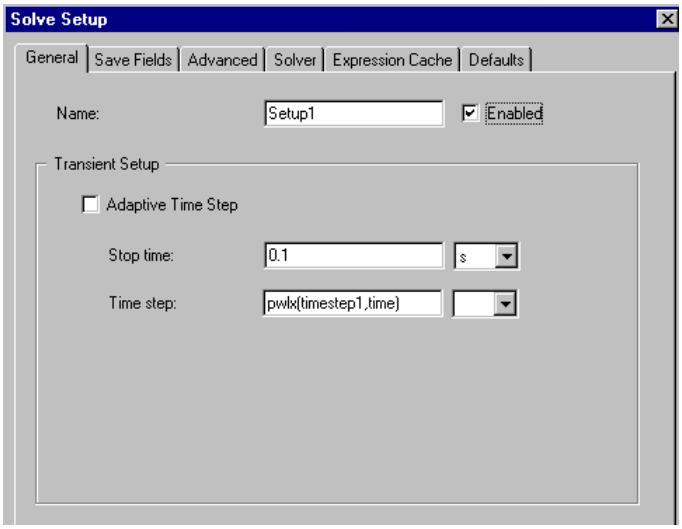

Figure A.2: Options available for the Analyse Setup. The stop time here is selected to 0.1 seconds, but is usually set depending on the number of periods to run, mechanical speed and number of polepairs. Timestep1 is the imported tab-file containing the constructed time vector.